



401 N. Lindbergh Blvd.
St. Louis, MO 63141
Tel.: 314.993.1700, #546
Toll Free: 800.424.2841, #546
Fax: 800.708.1364
Cell: 314.283.1983

Send via email to: jbode@aaortho.org and cyoung@aaortho.org

**AAO Foundation Final Report Form
(a/o 1/3/2018)**

Type of Award:

Biomedical Research Award – The 2017 Fred F. Schudy Memorial Research Award

Name(s) of Principal Investigator(s)

Noriaki Ono, DDS, PhD.
University of Michigan School of Dentistry, Department of Orthodontics & Pediatric Dentistry

Title of Project

Dynamic fates of resting chondrocytes in the cranial base synchondrosis

Period of AAOF Support (e.g. 07-01-18 to 06-30-19):

07-01-2017 to 06-30-2018

Amount of Funding

\$30,000

Summary/Abstract

The cranial base is central to craniofacial growth and determines the skeletal pattern of the face. Midfacial hypoplasia due to the cranial base deficiency is observed in many hereditary conditions affecting craniofacial growth, as well as in skeletal Class III populations. Currently, little is known about the mechanism underlying how the cranial base maintains its growth potential through development. Such fundamental knowledge is essential to predicting how individual genetic variants affect the growth pattern of the face.

The cranial base undergoes endochondral ossification and houses unique bidirectional growth plates termed the synchondroses. The cranial base synchondroses are structurally similar to the epiphyseal growth plates of long bones, and are composed of distinct layers of resting, proliferating and hypertrophic chondrocytes. Our laboratory has recently found that *growth-associated skeletal stem cells* (gSSCs) are formed among resting chondrocytes in the long bone epiphyseal growth plate. These cells differentiate into terminally differentiated chondrocytes, osteoblasts and bone marrow stromal cells, while also replicating themselves for long term presence within the growth plate. The objective of this project is to identify the fundamental characteristics of resting chondrocytes in the cranial base synchondrosis. **We hypothesize that resting chondrocytes of the cranial base synchondroses possess properties similar to those of long bone skeletal stem cells, and are essential for supporting cranial base growth.** Two specific aims in this project will provide the fundamental knowledge to support this hypothesis:

Aim 1. Define formation of resting chondrocytes in the cranial base synchondrosis.

Parathyroid hormone-related protein (PTHrP) is expressed by undifferentiated chondrocytes and delays their differentiation. PTHrP is therefore essential to maintenance of the growth plate. The working hypothesis of this proposal is that PTHrP-expressing resting chondrocytes are formed within the postnatal cranial base synchondrosis. Using *PTHrP*-mCherry knock-in fluorescent reporter mice we have generated, we will define the localization of *PTHrP*⁺ cranial base chondrocytes by analyzing serial sections of the synchondroses at various stages of development. Furthermore, we will identify slow-cycling chondrocytes among *PTHrP*⁺ chondrocytes (*PTHrP*⁺ resting chondrocytes) by taking advantage of serial injections of the thymidine analogue proliferation marker, EdU (5-ethynyl-2-deoxyuridine).

Aim 2. Determine cell fates of resting chondrocytes in the cranial base synchondrosis.

The working hypothesis is that resting chondrocytes in the synchondrosis behave as skeletal stem cells. To test this hypothesis, we will perform *in vivo* lineage-tracing experiments using a tamoxifen-inducible *PTHrP-creER* transgenic mouse line. Recombination in a *Rosa26*-tdTomato reporter locus results in permanent labeling of *PTHrP*⁺ cells, therefore their descendants can be traced. We will study how *PTHrP*⁺ resting chondrocytes establish columnar chondrocytes in the synchondroses, and differentiate into osteoblasts and bone marrow stromal cells in an adjacent region. In addition, we will define their self-renewal properties by chasing these cells for a long term to evaluate persistence or disappearance of tdTomato⁺ chondrocytes from the synchondroses. We will also reveal impact of these cells on cranial base growth by ablating *PTHrP*⁺ resting chondrocytes through an inducible diphtheria toxin fragment A (iDTA) allele.

These two aims will allow us to define the characteristics of resting chondrocytes in the cranial base synchondroses, and if these cells act as *skeletal stem cells* that play important roles in craniofacial growth and development. This study will deepen our understanding of the cranial base synchondroses as growth centers, and guide our future endeavor in facilitating personalized orthodontics to predict and modify craniofacial skeletal growth.

Detailed results and inferences:

Part of the funded project has been published in:

Mizuhashi K, Ono W, Matsushita Y, Sakagami N, Takahashi A, Saunders TL, Nagasawa T, Kronenberg HM, Ono N.

Resting zone of the growth plate harbors a unique class of skeletal stem cells.

Nature. 2018, 563(7730):254-258. PMID: 30401834

Please see the attached PDF file for more detail.

Response to the following questions:

1. Were the original, specific aims of the proposal realized?

A substantial proportion of the proposed project particularly regarding the cranial base is still actively being investigated. We expect that this project will be presented as an abstract in the 2020 IADR/AADR annual meeting in Washington DC.

A predoctoral student working on this project, Curtis Herzog, received a 2018 AADR Student Research Fellowship.

2. Were the results published?

a. If so, cite reference/s for publication/s including titles, dates, author or co-authors, journal, issue and page numbers

Mizuhashi K, Ono W, Matsushita Y, Sakagami N, Takahashi A, Saunders TL, Nagasawa T, Kronenberg HM, Ono N.

Resting zone of the growth plate houses a unique class of skeletal stem cells.

Nature. 2018, 563(7730):254-258. PMID: 30401834

b. Was AAOF support acknowledged?

Yes.

3. Have the results of this proposal been presented?

a. If so, list titles, author or co-authors of these presentation/s, year and locations

Ono N, Mizuhashi K, Kronenberg HM, Ono W.

Resting zone of the growth plate harbors a unique class of skeletal stem cells

2017 American Society for Bone and Mineral Research, 39th Annual Meeting, Denver.

b. Was AAOF support acknowledged?

Yes.

c. If not, are there plans to do so? If not, why not?

We plan to present more cranial based-focused aspects of this project for the 2020 IADR/AADR annual meeting in Washington DC. The first author will be Curtis Herzog.

4. To what extent have you used, or how do you intend to use, AAOF funding to further your career?

This AAOF funding indeed worked as an important bridge funding during the transition from the R00 grant to the R01 grant. We had a 5-month lapse in funding of the research grant as no-cost extension. Without this critical support from the AAOF, we would have been unable to sustain our research activities during the critical period leading up to publication.

Resting zone of the growth plate houses a unique class of skeletal stem cells

Koji Mizushima¹, Wanida Ono¹, Yuki Matsushita¹, Naoko Sakagami¹, Akira Takahashi¹, Thomas L. Saunders², Takashi Nagasawa³, Henry M. Kronenberg⁴ & Noriaki Ono^{1*}

Skeletal stem cells regulate bone growth and homeostasis by generating diverse cell types, including chondrocytes, osteoblasts and marrow stromal cells. The emerging concept postulates that there exists a distinct type of skeletal stem cell that is closely associated with the growth plate^{1–4}, which is a type of cartilaginous tissue that has critical roles in bone elongation⁵. The resting zone maintains the growth plate by expressing parathyroid hormone-related protein (PTHrP), which interacts with Indian hedgehog (Ihh) that is released from the hypertrophic zone^{6–10}, and provides a source of other chondrocytes¹¹. However, the identity of skeletal stem cells and how they are maintained in the growth plate are unknown. Here we show, in a mouse model, that skeletal stem cells are formed among PTHrP-positive chondrocytes within the resting zone of the postnatal growth plate. PTHrP-positive chondrocytes expressed a panel of markers for skeletal stem and progenitor cells, and uniquely possessed the properties of skeletal stem cells in cultured conditions. Cell-lineage analysis revealed that PTHrP-positive chondrocytes in the resting zone continued to form columnar chondrocytes in the long term; these chondrocytes underwent hypertrophy, and became osteoblasts and marrow stromal cells beneath the growth plate. Transit-amplifying chondrocytes in the proliferating zone—which was concertedly maintained by a forward signal from undifferentiated cells (PTHrP) and a reverse signal from hypertrophic cells (Ihh)—provided instructive cues to maintain the cell fates of PTHrP-positive chondrocytes in the resting zone. Our findings unravel a type of somatic stem cell that is initially unipotent and acquires multipotency at the post-mitotic stage, underscoring the malleable nature of the skeletal cell lineage. This system provides a model in which functionally dedicated stem cells and their niches are specified postnatally, and maintained throughout tissue growth by a tight feedback regulation system.

We first defined the formation of PTHrP⁺ chondrocytes in the growth plate using a *Pthrp-mCherry* (*Pthrp* is also known as *Pthlh*) knock-in reporter allele (Extended Data Fig. 1a, see also Supplementary Information). During the fetal stage, PTHrP-mCherry⁺ cells were mitotically active and localized within the Sox9⁺ perichondrial region (Extended Data Fig. 1b). Although this pattern continued at birth (Fig. 1a), a distinct group of PTHrP-mCherry⁺ chondrocytes appeared in the central area of the growth plate that is devoid of proliferation at postnatal day (P)3 (Extended Data Fig. 1c). These PTHrP-mCherry⁺ chondrocytes increased markedly in number between P6 and P9, and occupied a well-defined zone in the growth plate (Fig. 1b–d, Extended Data Fig. 1c); these chondrocytes were less proliferative than their counterparts in the proliferating zone (EdU⁺; 6.1 ± 2.3% of mCherry⁺ cells versus 30.5 ± 3.2% of proliferating chondrocytes at P9, *n* = 3 mice). Therefore, PTHrP-mCherry⁺ chondrocytes in the resting zone (‘resting chondrocytes’) develop in the postnatal growth plate, which is closely associated with the formation of secondary ossification centres. Flow cytometry analysis revealed that PTHrP-mCherry⁺ cells were exclusively found in the CD45^{neg} cell population in the

growth plate (Fig. 1e), and were completely absent in the CD45^{neg} population in bone and bone marrow cells (Extended Data Fig. 2a). PTHrP-mCherry⁺ cells in the growth plate did not express Col1a1(2.3kb)-GFP (Extended Data Fig. 2b), which indicates that PTHrP-mCherry is specifically expressed by growth-plate chondrocytes but not by osteoblasts or bone marrow stromal cells. We next asked whether PTHrP-mCherry⁺ resting chondrocytes express a panel of cell-surface markers for transplantable skeletal stem and progenitor cells³—particularly three subsets of skeletal stem and progenitor populations (integrin alpha V (CD51)⁺Thy-1 (CD90)⁻; mouse skeletal stem cells (mSSCs) (CD105⁻CD200⁺), pre-bone, cartilage and stromal progenitors (pre-BCSPs) (CD105⁻CD200⁻), and bone, cartilage and stromal progenitors (BCSPs) (CD105⁺). A large majority of CD45⁻Ter119⁻CD31⁻ growth-plate cells—including both mCherry⁻ and mCherry⁺ fractions—were in a CD51⁺CD90⁻ skeletal stem and progenitor population (Fig. 1f, left panels). Among CD45⁻Ter119⁻CD31⁻CD51⁺CD90⁻ mCherry⁺ cells, 49.2 ± 8.4%, 23.4 ± 8.4% and 27.4 ± 16.5% were CD105⁻CD200⁺ (mSSCs), CD105⁻CD200⁻ (pre-BCSPs) and CD105⁺ (BCSPs), respectively (Fig. 1f, right panels; see also Extended Data Fig. 2c, d). Conversely, 41.6 ± 4.4%, 31.7 ± 6.2% and 53.4 ± 16.9% of mSSCs, pre-BCSPs and BCSPs, respectively, were positive for PTHrP-mCherry (Extended Data Fig. 2e). Therefore, PTHrP-mCherry⁺ resting chondrocytes represent a substantial subset of immunophenotypically defined skeletal stem and progenitor cells in the growth plate.

We next determined whether PTHrP⁺ resting chondrocytes behave as stem cells *in vivo*, by using a *Pthrp-creER* bacterial artificial chromosome transgenic line (L909, Extended Data Fig. 3a; see also Supplementary Information, Supplementary Methods and Extended Data Fig. 10 for establishment of this system and validation of tamoxifen-negative controls). Analysis of *Pthrp*^{mCherry/+}; *Pthrp-creER*; *R26R*^{ZsGreen} mice revealed that ZsGreen⁺ cells largely overlapped with mCherry⁺ cells shortly after a tamoxifen pulse at P6 (Extended Data Fig. 3b–d). The percentage of CD105⁺ cells within the ZsGreen⁺ cell population was significantly lower than that within the mCherry⁺ cell population (Extended Data Fig. 3e), which indicates that *Pthrp-creER* preferentially marks an immature subset of PTHrP-mCherry⁺ cells. An EdU label-exclusion assay of *Pthrp-creER*; *R26R*^{tdTomato} mice pulsed with tamoxifen at P6 revealed that a large majority of tdTomato⁺ cells were resistant to EdU incorporation (Extended Data Fig. 3f, EdU⁺; 7.7 ± 2.0% of tdTomato⁺ cells versus 61.1 ± 11.5% of proliferating-zone chondrocytes, *n* = 3 mice), which demonstrates that *Pthrp-creER* specifically marks resting chondrocytes (Extended Data Fig. 3g). These PTHrP⁺ resting chondrocytes did not express Grem1⁴ (Extended Data Fig. 3h). Subsequently, we traced the fate of PTHrP⁺ resting chondrocytes labelled on P6 (hereafter, PTHrP^{CE}-P6 cells) *in vivo*. After remaining within the resting zone at P12 (Fig. 2a; see also Extended Data Fig. 3g), PTHrP^{CE}-P6 cells first formed short columns (composed of <10 cells) (Fig. 2b, arrowhead) and subsequently formed longer columns (composed of >10 cells) that originated from the

¹University of Michigan School of Dentistry, Ann Arbor, MI, USA. ²Transgenic Animal Model Core, University of Michigan Medical School, Ann Arbor, MI, USA. ³Laboratory of Stem Cell Biology and Developmental Immunology, Graduate School of Frontier Biosciences, Osaka University School of Medicine, Suita, Japan. ⁴Endocrine Unit, Massachusetts General Hospital and Harvard Medical School, Boston, MA, USA. *e-mail: noriono@umich.edu

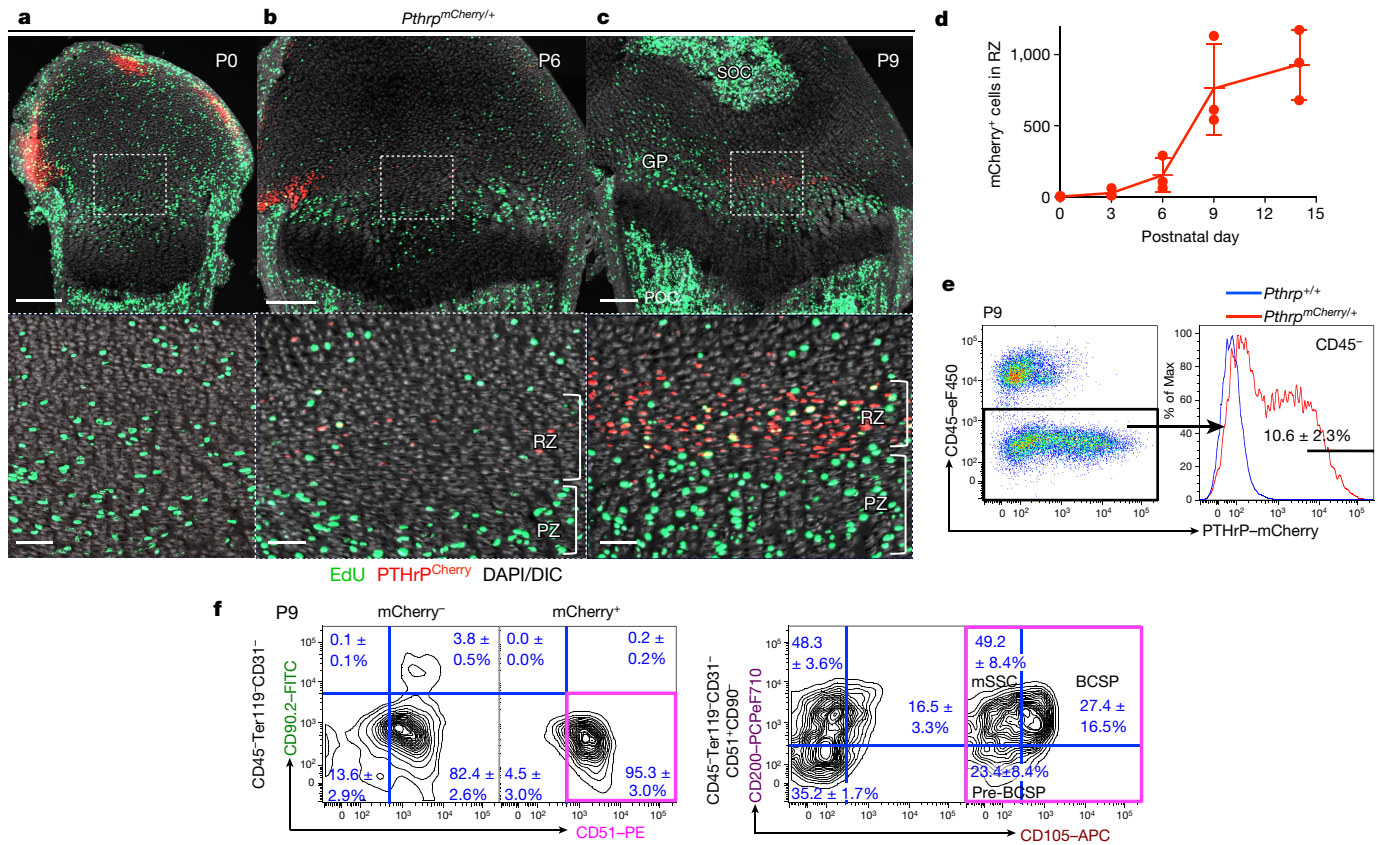


Fig. 1 | Formation of PTHrP-mCherry⁺ chondrocytes in the resting zone of the growth plate. **a–c**, *Pthrp*^{mCherry/+} distal-femur growth plates with EdU administration shortly before analysis. Bottom panels show magnified views of central growth plates. RZ, resting zone; PZ, proliferating zone; GP, growth plate; POC, primary ossification centre; SOC, secondary ossification centre. Grey, DAPI and DIC. Scale bars, 200 μ m (top panels), 50 μ m (bottom panels). **d**, Quantification of mCherry⁺ cells. $n = 3$ mice per group, data are presented as

mean \pm s.d. **e**, Flow cytometry analysis of *Pthrp*^{mCherry/+} growth-plate cells. $n = 8$ mice, data are presented as mean \pm s.d. **f**, Skeletal stem and progenitor cell-surface-marker analysis of *Pthrp*^{mCherry/+} growth-plate cells. mCherry⁻, mCherry⁺ fraction of *Pthrp*^{mCherry/+} cells; mCherry⁺, mCherry⁺ fraction of *Pthrp*^{mCherry/+} cells. Magenta box, CD45⁻Ter119⁻CD31⁻CD51⁺CD90⁻mCherry⁺ fraction. $n = 3$ mice per group, data are presented as mean \pm s.d.

resting zone, at around P18 (Fig. 2c, arrows). After a month of chase, PTHrP^{CE}-P6 cells constituted the entire column from the resting zone to the hypertrophic zone (Fig. 2d). The number of tdTomato⁺ resting chondrocytes transiently increased during the first week of chase and decreased thereafter, owing to the formation of columnar chondrocytes (Fig. 2e). The number of short tdTomato⁺ columns peaked at P18 and decreased thereafter, whereas long tdTomato⁺ columns appeared at P18 and continued to increase until P36 (Fig. 2f). Thus, *Pthrp-creER*⁺ resting chondrocytes stay within the resting zone for the first week, and establish columnar chondrocytes starting from the second week of chase. Analysis of *Pthrp-creER*;*R26R*^{Confetti} mice revealed that each column was marked by its unique colour (CFP, YFP or tdTomato, Fig. 2g), which demonstrates that single *Pthrp-creER*⁺ resting chondrocytes can give rise to multiple types of chondrocytes. Additional analysis of *Col2a1-creER*;*R26R*^{Confetti} mice further supported the existence of clonal cell populations (Extended Data Fig. 4a). Together, these findings support the notion that individual PTHrP⁺ resting chondrocytes are multipotent and can clonally establish columnar chondrocytes in the growth plate.

To investigate whether *Pthrp-creER*⁺ resting chondrocytes undergo self-renewing asymmetric divisions, we performed an EdU label-retention assay. Analysis of PTHrP^{CE}-P6 cells with serial pulses of EdU revealed that, after three weeks of chase, these cells gradually diluted the EdU signal as they differentiated towards the hypertrophic zone (Fig. 2h). Further, PTHrP^{CE}-P6 cells in the resting zone expressed PTHrP-mCherry, whereas those in the proliferating zone lost this expression (Fig. 2i). Therefore, *Pthrp-creER*⁺ chondrocytes maintain themselves in the resting zone as PTHrP⁺ cells and become the

source of columnar chondrocytes in the growth plate, by providing the transit-amplifying progeny. Analysis of *Pthrp-creER*;*R26R*^{tdTomato} mice after being pulsed at various preceding pre-natal and early post-natal time points revealed that *Pthrp-creER*⁺ chondrocytes started to be formed within the resting zone at embryonic day (E)17.5 (Extended Data Fig. 4b–e); a tamoxifen pulse on a later day laterally expanded the domain of tdTomato⁺ cells. However, once they were marked, tdTomato⁺ cells did not expand laterally upon further chase (Extended Data Fig. 4f,g), which indicates that PTHrP⁺ resting chondrocytes are dedicated—at least to some degree—to making columnar chondrocytes longitudinally. Additional analysis of *Dlx5-creER*;*R26R*^{tdTomato} mice revealed that chondrocytes in the proliferating and hypertrophic zone could only form short columns (<10 cells) that eventually disappeared from the growth plate (Extended Data Fig. 5a–d), indicating that *Dlx5-creER*⁺ proliferating chondrocytes are not the source of columnar chondrocytes in the growth plate.

During an extended chase period, PTHrP^{CE}-P6 cells continued to form columnar chondrocytes within the growth plate for at least a year after the pulse (Fig. 3a–c for *Col1a1(2.3kb)-GFP*; Extended Data Fig. 6a–d for *Cxcl12-GFP*¹²): the number of tdTomato⁺ columns in the growth plate gradually decreased until six months after the pulse, and reached a plateau thereafter (Fig. 3d). A majority of tdTomato⁺ columns extended beyond the hypertrophic layer and continued into the primary spongiosa and the metaphyseal bone marrow, an area beneath the growth plate¹³. These chondrocytes became *Cxcl12-GFP*⁺ stromal cells beneath tdTomato⁺ columns (Extended Data Fig. 6e), and reticular cells near trabecular bones (Fig. 3a, bottom). These chondrocytes also became *Col1a1(2.3kb)-GFP*⁺ osteoblasts on the trabecular surface

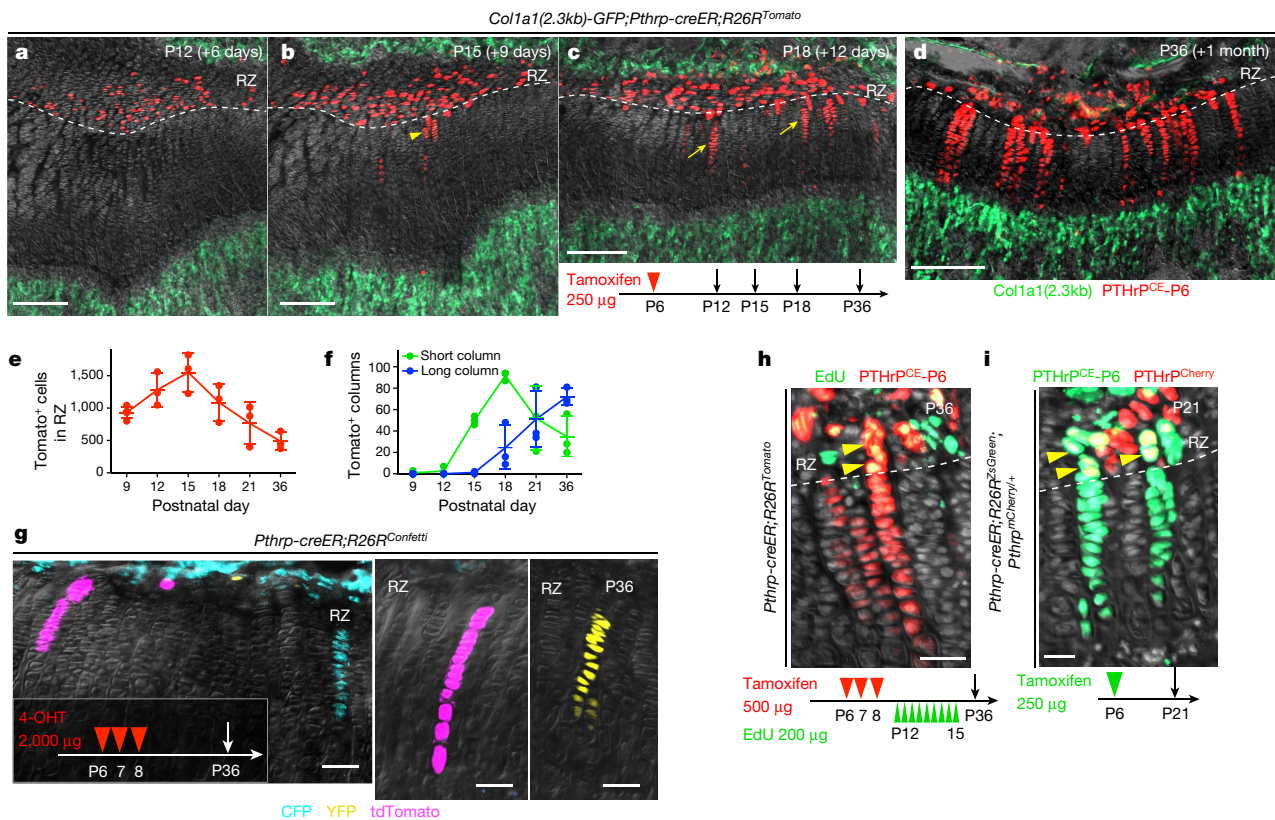


Fig. 2 | *Pthrp-creER*⁺ resting chondrocytes are the source of columnar chondrocytes. **a–d**, Cell-fate analysis of *Pthrp-creER*⁺ resting chondrocytes. *Col1a1(2.3kb)-GFP;Pthrp-creER;R26R^{tdTomato}* (pulsed on P6) distal-femur growth plates. Arrowhead, short column (<10 cells); arrows, long columns (>10 cells). Scale bars, 200 μ m. **e, f**, Quantification of tdTomato⁺ cells in resting zone (red line) (**e**) and columns in growth plate, short columns (<10 cells, green line) and long columns (>10 cells, blue line) (**f**). $n = 5$ (P9), $n = 3$ (P12–P36) mice per group, data are presented as mean \pm s.d. **g**, In vivo clonal analysis of *Pthrp-creER*⁺

resting chondrocytes. *Pthrp-creER;R26R^{Confetti}* distal-femur growth plates (pulsed on P6, P7 and P8). 4-OHT, 4-hydroxytamoxifen. Scale bars, 50 μ m. $n = 3$ mice. **h**, EdU label-retention assay of *Pthrp-creER;R26R^{tdTomato}* distal-femur growth plates (pulsed on P6, P7 and P8). Arrowheads, EdU-retaining tdTomato⁺ cells. Scale bars, 50 μ m. $n = 3$ mice. **i**, PTHrP-mCherry expression in *Pthrp-creER;R26R^{ZsGreen};Pthrp^{mCherry/+}* distal-femur growth plates (pulsed on P6). Arrowheads, PTHrP-mCherry⁺ZsGreen⁺ cells. Scale bars, 20 μ m. Grey, DAPI and DIC. $n = 3$ mice.

(Fig. 3a, bottom) and in the primary spongiosa (Fig. 3b, bottom). The number of Cxcl12-GFP⁺tdTomato⁺ stromal cells and Col1a1(2.3kb)-GFP⁺tdTomato⁺ osteoblasts increased for the first three months of chase; subsequently, the number of Col1a1(2.3kb)-GFP⁺tdTomato⁺ osteoblasts decreased, whereas the number of Cxcl12-GFP⁺tdTomato⁺ stromal cells reached a plateau (Fig. 3e). These cells did not become bone marrow adipocytes in the presence of a high-fat diet that contained a PPAR- γ agonist rosiglitazone (LipidTOX⁺, 0 out of 443 cells examined; Extended Data Fig. 6f). Therefore, a subset of *Pthrp-creER*⁺ resting chondrocytes can continue to reproduce themselves within the resting zone in the long term; their descendants first differentiate into hypertrophic chondrocytes within the growth plate, and then become multiple types of cells beyond the growth plate, such as osteoblasts and bone marrow stromal cells—but not adipocytes—in vivo.

We next performed a colony-forming assay to test whether *Pthrp-creER*⁺ resting chondrocytes behave as skeletal stem cells in cultured conditions^{14,15}. PTHrP^{CE}-P6 cells formed distinct and large tdTomato⁺ colonies (>50 cells) composed of small Sox9⁺ spherical cells (about 20 μ m in diameter) (Extended Data Fig. 7a, b). By contrast, Dlx5⁺ proliferating chondrocytes labelled on P7 failed to form tdTomato⁺ colonies (Extended Data Fig. 7b, right), which indicates that *Pthrp-creER*⁺ resting chondrocytes uniquely possess the capacity to form colonies when cultured ex vivo (Extended Data Fig. 7c). We next isolated individual primary PTHrP^{CE}-tdTomato⁺ colonies and sub-cultured them further to determine whether individual colony-forming cells can self-renew in vitro (Extended Data Fig. 7d, see also Supplementary Information). Although a small fraction of P9 PTHrP^{CE}-tdTomato⁺ primary colonies had the ability to establish secondary colonies

(17 out of 518 clones, 3.3%), none of them could survive a further passage (Extended Data Fig. 7e). By contrast, an increased fraction of P12 PTHrP^{CE}-tdTomato⁺ colonies established secondary colonies (16 out of 98 clones, 16.3%), and a fraction of these clones (2 out of 16 clones, 12.5%) could be further passaged for at least nine generations (Fig. 4a). Thus, *Pthrp-creER*⁺ colony-forming cells appear to acquire robust in vitro self-renewability when the secondary ossification centre actively develops. Further, individual PTHrP^{CE}-tdTomato⁺ cells (passage 4–7) could generate Alcian blue⁺ spheres, Alizarin red⁺ mineralized matrix and LipidTOX⁺ oil droplets under chondrogenic, osteogenic and adipogenic differentiation conditions, respectively (Figs. 4b, 4 out of 4 clones, 100%). Upon subcutaneous transplantation into immunodeficient mice, these cells robustly differentiated into Col1a1(2.3kb)-GFP⁺ osteoblastic cells (Fig. 4c) and effectively gave rise to Alcian blue⁺ and Alizarin red⁺ matrix, but produced Oil red O⁺ lipid droplets only ineffectively (Extended Data Fig. 7f). These findings indicate that PTHrP⁺ skeletal stem cells are predisposed to become chondrocytes and osteoblasts in vivo, and possess a baseline potential to become adipocytes in an inductive condition in vitro.

Lastly, we set out to investigate the functional importance of PTHrP⁺ resting chondrocytes. Inducible cell ablation experiments using *Pthrp-creER;R26^{Isl-tdTomato/+}* (control) and *Pthrp-creER;R26^{Isl-tdTomato/iDTA}* (hereafter, DTA) littermates revealed that *Pthrp-creER*⁺ cells were only incompletely ablated; tdTomato⁺ resting chondrocytes and columns were still observed in the induced tissue of DTA mice (Fig. 5a, b). Nonetheless, the height of each layer of the growth plate was altered in the induced tissue of DTA mice, in which the proliferating zone was significantly reduced in association with the

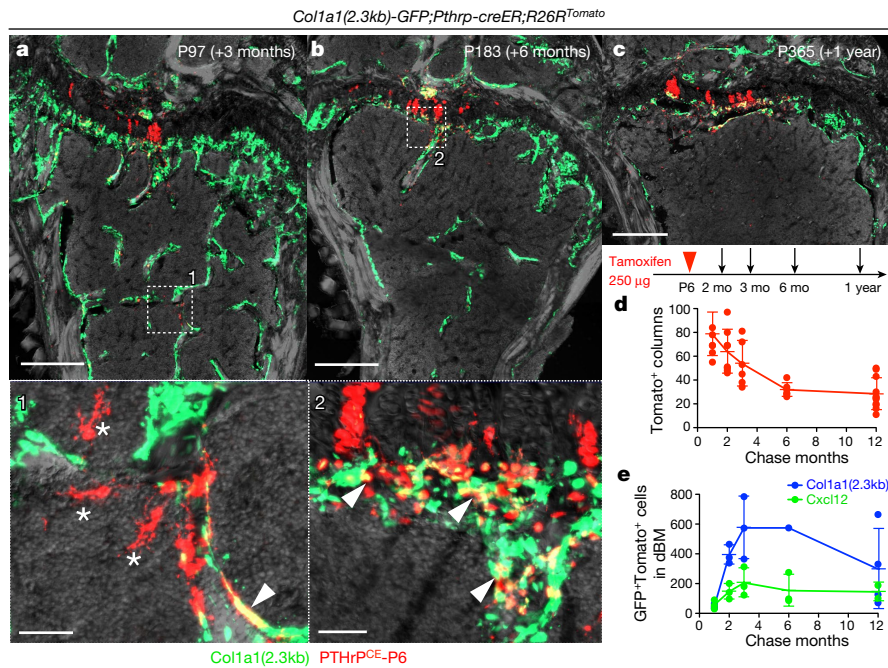


Fig. 3 | *Pthrp-creER*⁺ resting chondrocytes behave as skeletal stem cells in vivo. **a–c**, Long-chase analysis of *Pthrp-creER*⁺ resting chondrocytes. *Col1a1(2.3kb)-GFP;Pthrp-creER;R26R^{tdTomato}* distal femurs (pulsed on P6). In **a**, **b**, the bottom panel shows a magnified view of marrow space (white box in top panel). Arrowheads, Col1a1(2.3kb)-GFP⁺tdTomato⁺ osteoblasts; asterisks, tdTomato⁺ reticular stromal cells. Grey, DAPI and DIC. Scale bars, 500 μ m (top panels), 50 μ m (bottom panels). $n = 3$ mice per group, except in **b**, $n = 1$ mouse. **d**, Quantification of tdTomato⁺ columns in growth plate (red line) during the chase. $n = 8$ (1 month,

2 months), $n = 6$ (3 months, 6 months), $n = 11$ (12 months) mice per group, data are presented as mean \pm s.d. **e**, Quantification of Col1a1(2.3kb)-GFP⁺tdTomato⁺ osteoblasts (blue line) and Cxcl12-GFP⁺tdTomato⁺ stromal cells (green line) in distal bone and bone marrow (dBM, up to 5 mm from the growth plate) during the chase. $n = 3$ (1 month, 2 months, 3 months for Col1a1(2.3kb)-GFP and Cxcl12-GFP, 6 months for Cxcl12-GFP), $n = 4$ (12 months for Col1a1(2.3kb)-GFP), $n = 2$ (12 months for Cxcl12-GFP) mice per group, data are presented as mean \pm s.d., $n = 1$ (6 months for Col1a1(2.3kb)-GFP) mouse.

significant expansion of the hypertrophic and resting zones (Fig. 5c). Therefore, partial loss of PTHrP⁺ cells in the resting zone is sufficient to alter the integrity of the growth plate by inducing premature hypertrophic differentiation of chondrocytes in the proliferating zone.

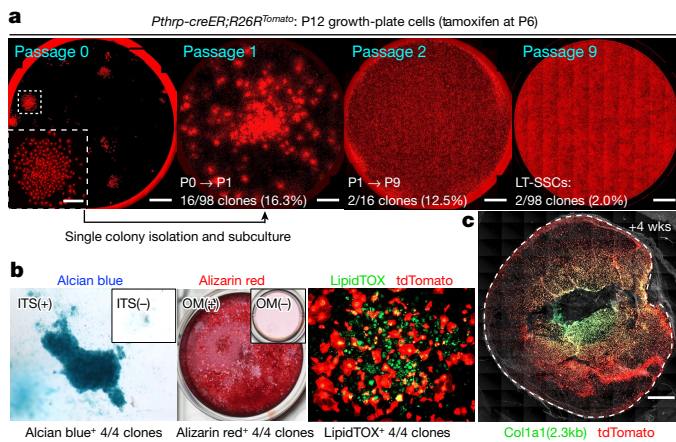


Fig. 4 | Skeletal stem cell activities of *Pthrp-creER*⁺ resting chondrocytes ex vivo. **a**, Colony-forming assay and subsequent passaging of individual PTHrP^{CE}-tdTomato⁺ colonies. Inset, magnified view of single colony. Red, tdTomato. Scale bars, 5 mm, 1 mm (inset). LT-SSCs, long-term skeletal stem cells. $n = 98$ independent experiments. **b**, Trilineage differentiation of PTHrP^{CE}-tdTomato⁺ clones (passage 4 to 7). Chondrogenic (left), osteogenic (centre) and adipogenic (right) differentiation conditions. Insets, differentiation-medium negative controls. ITS, insulin-transferrin-selenium, OM, osteogenic differentiation medium. Four independent clones were tested. **c**, Subcutaneous transplantation of PTHrP^{CE}-tdTomato⁺ clones into immunodeficient mice. Dotted line, contour of the plug. Grey, DIC. Scale bars, 1 mm. $n = 8$ mice.

Moreover, global manipulation of Hedgehog (Hh) signalling using Smo agonist (SAG) and antagonist (LDE225) in *Pthrp-creER;R26R^{tdTomato}* mice pulsed on P6 revealed that these regimens predominantly affected chondrocytes in the proliferating zone, without directly affecting PTHrP^{CE}-P6 cells in the resting zone (Extended Data Fig. 8a–c). Both regimens resulted in a significantly reduced number of tdTomato⁺ columns (Fig. 5d; see also Extended Data Fig. 8d–k), indicating that uninterrupted Hh signalling is essential to maintaining the proper cell fates of PTHrP⁺ resting chondrocytes. *Pthrp-creER*⁺ cells directly differentiated into Col1a1(2.3kb)-GFP⁺ osteoblasts in response to micro-perforation injury (Extended Data Fig. 8l, m), which indicates that PTHrP⁺ skeletal stem cells lose their physiological fate in the absence of an intact proliferating zone.

Here we identified that the resting zone of the growth plate houses a unique class of skeletal stem cells, the transit-amplifying progeny of which are lineage-restricted as chondrocytes that exhibit multipotency only at the post-mitotic stage (see Extended Data Fig. 9a, b). PTHrP⁺ cells are one of the stem-cell subgroups organized within the resting zone and—together with other as-yet unidentified cells—these cells can concertedly contribute to long-term tissue renewal. PTHrP⁺ skeletal stem cells are dedicated to making columnar chondrocytes longitudinally, and appear to derive from PTHrP⁻ cells. PTHrP⁺ stem cells are highly hierarchical; approximately 2–3% of these cells acquire long-term self-renewability (Extended Data Fig. 9b). In addition, these stem cells are endowed with the ability to maintain the integrity of the growth plate, by sending a forward signal (that is, PTHrP) for transit-amplifying chondrocytes to maintain their proliferation and delay their hypertrophy in a non-cell autonomous manner. Therefore, PTHrP⁺ stem cells can also provide the niche for transit-amplifying cells, which is compatible with a model previously proposed for the epithelium¹⁶. Conversely, transit-amplifying cells—which are maintained in a Hedgehog-responsive manner—appear to provide instructive cues to determine the cell fates of PTHrP⁺ stem cells within the growth

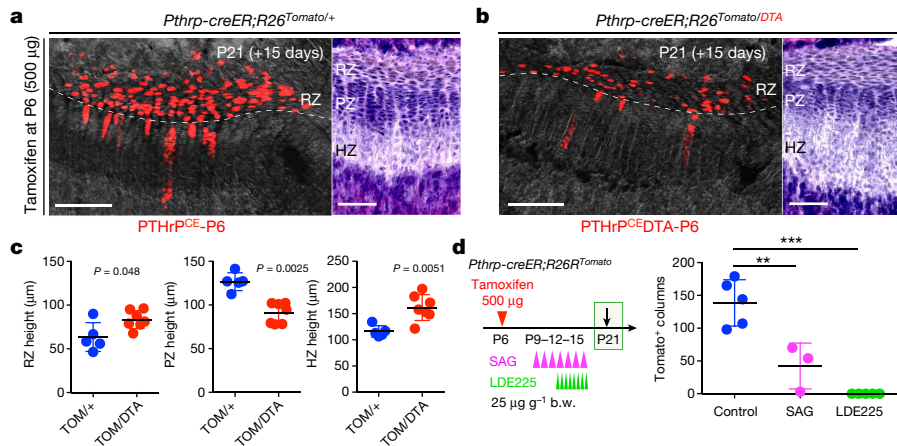


Fig. 5 | Reciprocal interactions between PTHrP-creER⁺ resting chondrocytes and their niche. **a–c**, DTA-mediated ablation of *Pthrp-creER⁺* resting chondrocytes. **a**, *Pthrp-creER;R26^{Isl-tdTomato/+}* (control). **b**, *Pthrp-creER;R26^{Isl-tdTomato/DTA}* (DTA) distal-femur growth plates (pulsed on P6). HZ, hypertrophic zone. Grey, DAPI and DIC. Right panels, haematoxylin and eosin staining. Scale bars, 200 µm (left panels) and 100 µm (right panels). **c**, Quantification of resting (left), proliferating (centre) and hypertrophic (right) zone height. TOM, tdTomato. $n = 5$ mice for control, $n = 7$ mice for DTA, data are presented as mean \pm s.d., P values from Mann–Whitney’s U -test, two-tailed. **d**, Pharmacological

manipulation of Hedgehog signalling. Quantification of tdTomato⁺ columns in *Pthrp-creER;R26^{Isl-tdTomato}* distal-femur growth plates (pulsed on P6). $n = 5$ (control), $n = 3$ (SAG) and $n = 5$ (LDE225) mice per group, data are presented as mean \pm s.d., $**P < 0.01$, $***P < 0.001$. Control versus SAG, mean difference = 96.2, 95% confidence interval (41.6, 150.9); control versus LDE225, mean difference = 138.6, 95% confidence interval (91.3, 185.9); SAG versus LDE225, mean difference = 42.3, 95% confidence interval (–12.3, 97.0). One-way ANOVA followed by Tukey’s multiple comparison test. b.w., body weight.

plate, which implies a reciprocal interaction between the stem cells and their progeny. We assume that PTHrP[–] short-term precursors are the principal driver for extensive bone growth that occurs during postnatal development, reminiscent of a model proposed for haematopoietic stem cells^{17,18}. It is possible that PTHrP⁺ skeletal stem cells are mainly involved in the long-term maintenance of skeletal integrity, although further details need to be clarified.

Data availability

Source Data are provided in the online version of the paper. The datasets generated during and/or analysed during the current study are available in Dryad Digital Repository (<https://doi.org/10.5061/dryad.3qq5bm7>).

Online content

Any methods, additional references, Nature Research reporting summaries, source data, statements of data availability and associated accession codes are available at <https://doi.org/10.1038/s41586-018-0662-5>.

Received: 23 September 2017; Accepted: 10 September 2018;
 Published online: 31 October 2018

- Ono, N. & Kronenberg, H. M. Bone repair and stem cells. *Curr. Opin. Genet. Dev.* **40**, 103–107 (2016).
- Ono, N., Ono, W., Nagasawa, T. & Kronenberg, H. M. A subset of chondrogenic cells provides early mesenchymal progenitors in growing bones. *Nat. Cell Biol.* **16**, 1157–1167 (2014).
- Chan, C. K. et al. Identification and specification of the mouse skeletal stem cell. *Cell* **160**, 285–298 (2015).
- Worthley, D. L. et al. Gremlin 1 identifies a skeletal stem cell with bone, cartilage, and reticular stromal potential. *Cell* **160**, 269–284 (2015).
- Kronenberg, H. M. Developmental regulation of the growth plate. *Nature* **423**, 332–336 (2003).
- St-Jacques, B., Hammerschmidt, M. & McMahon, A. P. Indian hedgehog signaling regulates proliferation and differentiation of chondrocytes and is essential for bone formation. *Genes Dev.* **13**, 2072–2086 (1999).
- Kobayashi, T. et al. PTHrP and Indian hedgehog control differentiation of growth plate chondrocytes at multiple steps. *Development* **129**, 2977–2986 (2002).
- Kobayashi, T. et al. Indian hedgehog stimulates periarticular chondrocyte differentiation to regulate growth plate length independently of PTHrP. *J. Clin. Invest.* **115**, 1734–1742 (2005).
- Chen, X. et al. Initial characterization of PTH-related protein gene-driven lacZ expression in the mouse. *J. Bone Miner. Res.* **21**, 113–123 (2006).
- Mak, K. K., Kronenberg, H. M., Chuang, P. T., Mackem, S. & Yang, Y. Indian hedgehog signals independently of PTHrP to promote chondrocyte hypertrophy. *Development* **135**, 1947–1956 (2008).
- Abad, V. et al. The role of the resting zone in growth plate chondrogenesis. *Endocrinology* **143**, 1851–1857 (2002).

- Ara, T. et al. A role of CXC chemokine ligand 12/stromal cell-derived factor-1/pre-B cell growth stimulating factor and its receptor CXCR4 in fetal and adult T cell development in vivo. *J. Immunol.* **170**, 4649–4655 (2003).
- Yang, L., Tsang, K. Y., Tang, H. C., Chan, D. & Cheah, K. S. Hypertrophic chondrocytes can become osteoblasts and osteocytes in endochondral bone formation. *Proc. Natl Acad. Sci. USA* **111**, 12097–12102 (2014).
- Bianco, P. et al. The meaning, the sense and the significance: translating the science of mesenchymal stem cells into medicine. *Nat. Med.* **19**, 35–42 (2013).
- Bianco, P. ‘Mesenchymal’ stem cells. *Annu. Rev. Cell Dev. Biol.* **30**, 677–704 (2014).
- Pardo-Saganta, A. et al. Parent stem cells can serve as niches for their daughter cells. *Nature* **523**, 597–601 (2015).
- Sun, J. et al. Clonal dynamics of native haematopoiesis. *Nature* **514**, 322–327 (2014).
- Busch, K. et al. Fundamental properties of unperturbed haematopoiesis from stem cells in vivo. *Nature* **518**, 542–546 (2015).

Acknowledgements We thank D. Holcomb and M. Curtis of Carl Zeiss Microscopy for assistance in imaging, G. Gavrilina and W. Fillipak of the University of Michigan Transgenic Animal Model Core for assistance with transgenesis. This research was supported by NIH R01DE026666 and R00DE022564 (to N.O.), R03DE027421 (to W.O.), P01DK011794 (to H.M.K.), 2017 Fred F. Schudy Memorial Research Award from the American Association of Orthodontists Foundation (to N.O.) and University of Michigan MCUBed 2.0 Grant (to N.O. and W.O.).

Reviewer information Nature thanks O. Klein, M. T. Longaker and the other anonymous reviewer(s) for their contribution to the peer review of this work.

Author contributions K.M. and N.O. conceived the project and designed the experiments; K.M. and N.O. performed the mouse genetic experiments with assistance from W.O., N.S. and A.T., who performed genotyping; K.M. performed histological experiments and imaging analysis; K.M. performed cell culture experiments; K.M. and N.O. performed flow cytometry experiments and analysis; Y.M. performed the surgery and cell transplantation; K.M. and N.O. analysed the data; N.O. supervised the project; T.L.S. generated the mice; T.N. provided the mice; K.M. and N.O. wrote the manuscript; T.N., W.O. and H.M.K. critiqued the manuscript.

Competing interests The authors declare no competing interests.

Additional information

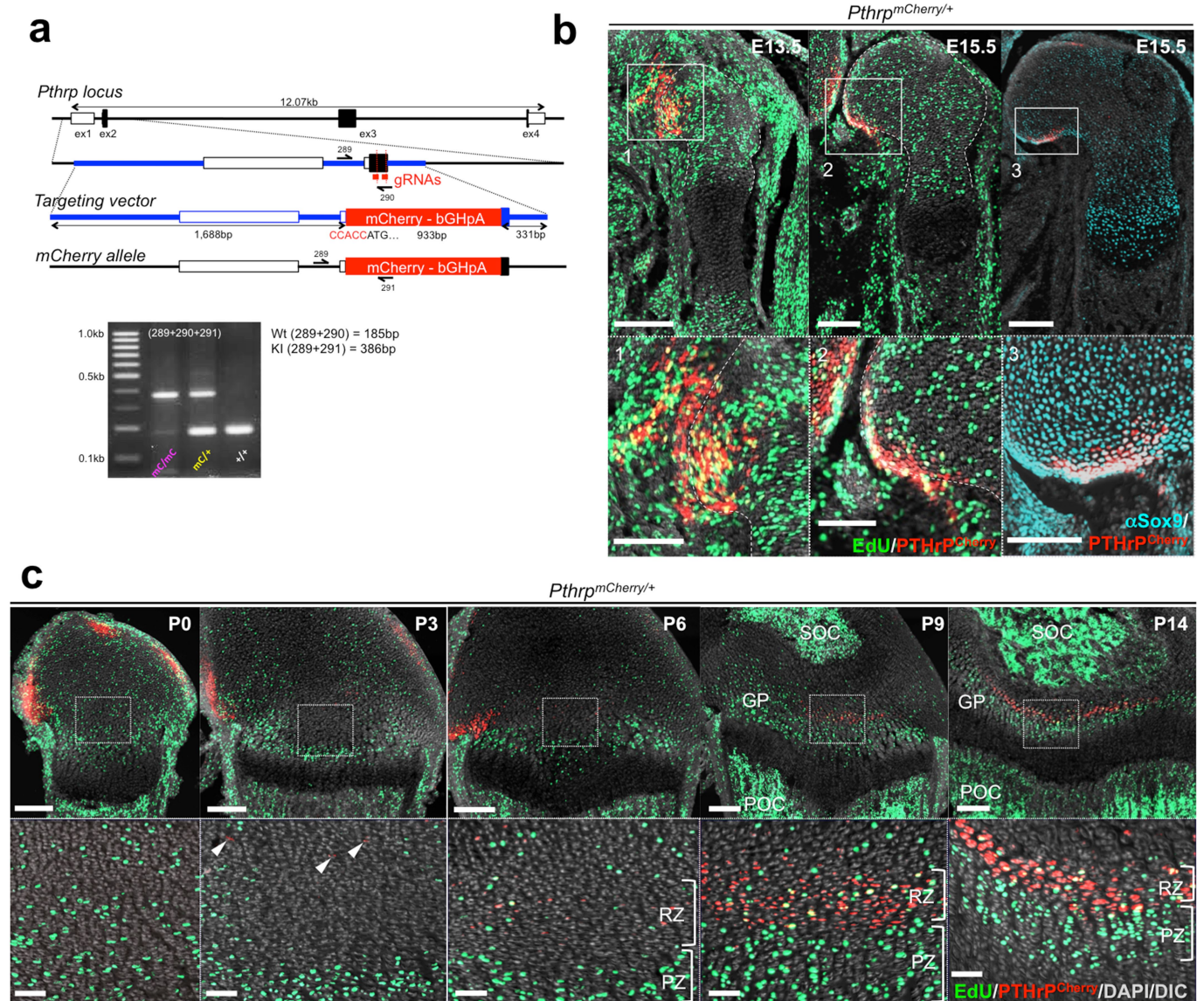
Extended data is available for this paper at <https://doi.org/10.1038/s41586-018-0662-5>.

Supplementary information is available for this paper at <https://doi.org/10.1038/s41586-018-0662-5>.

Reprints and permissions information is available at <http://www.nature.com/reprints>.

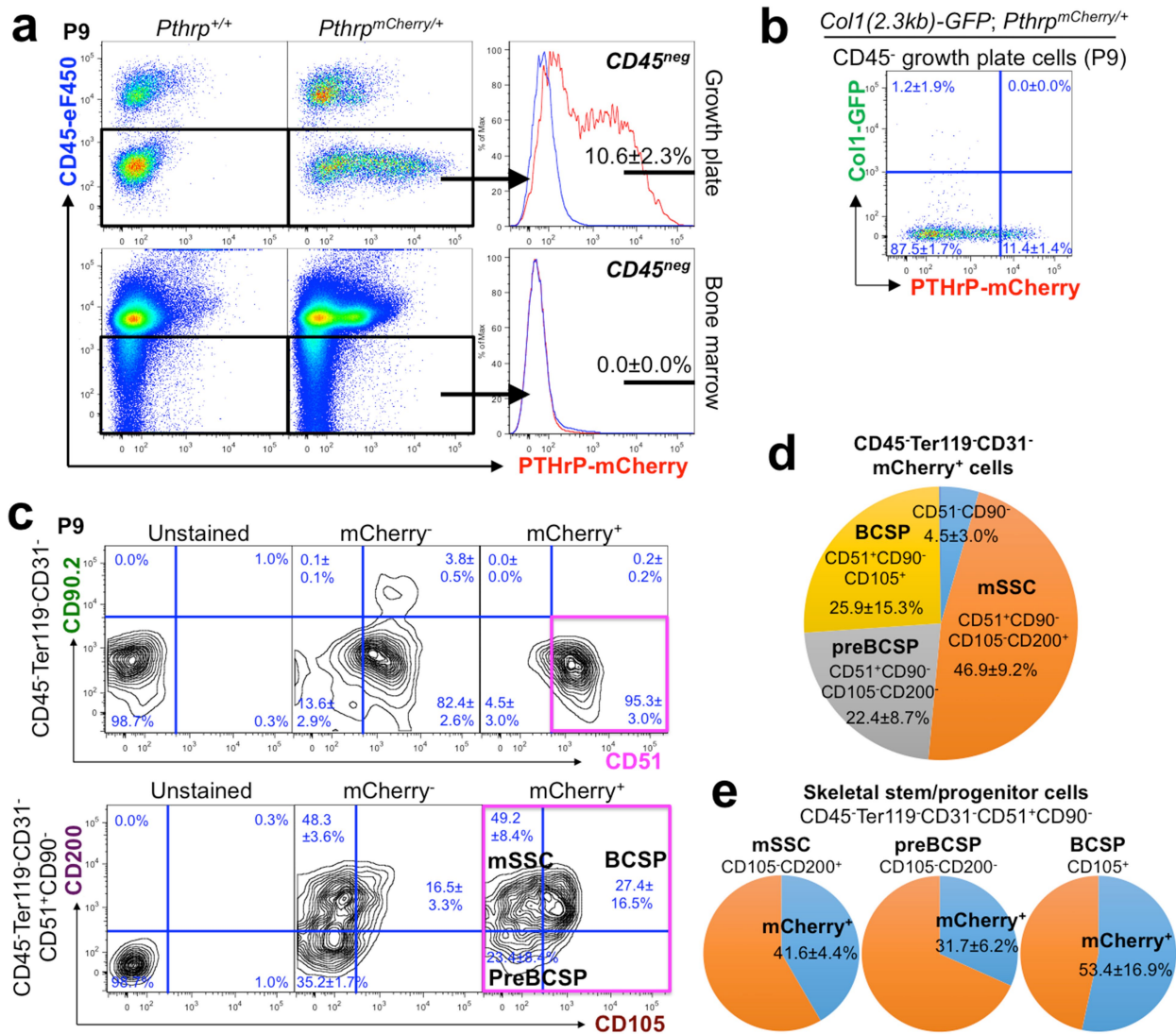
Correspondence and requests for materials should be addressed to N.O.

Publisher’s note: Springer Nature remains neutral with regard to jurisdictional claims in published maps and institutional affiliations.



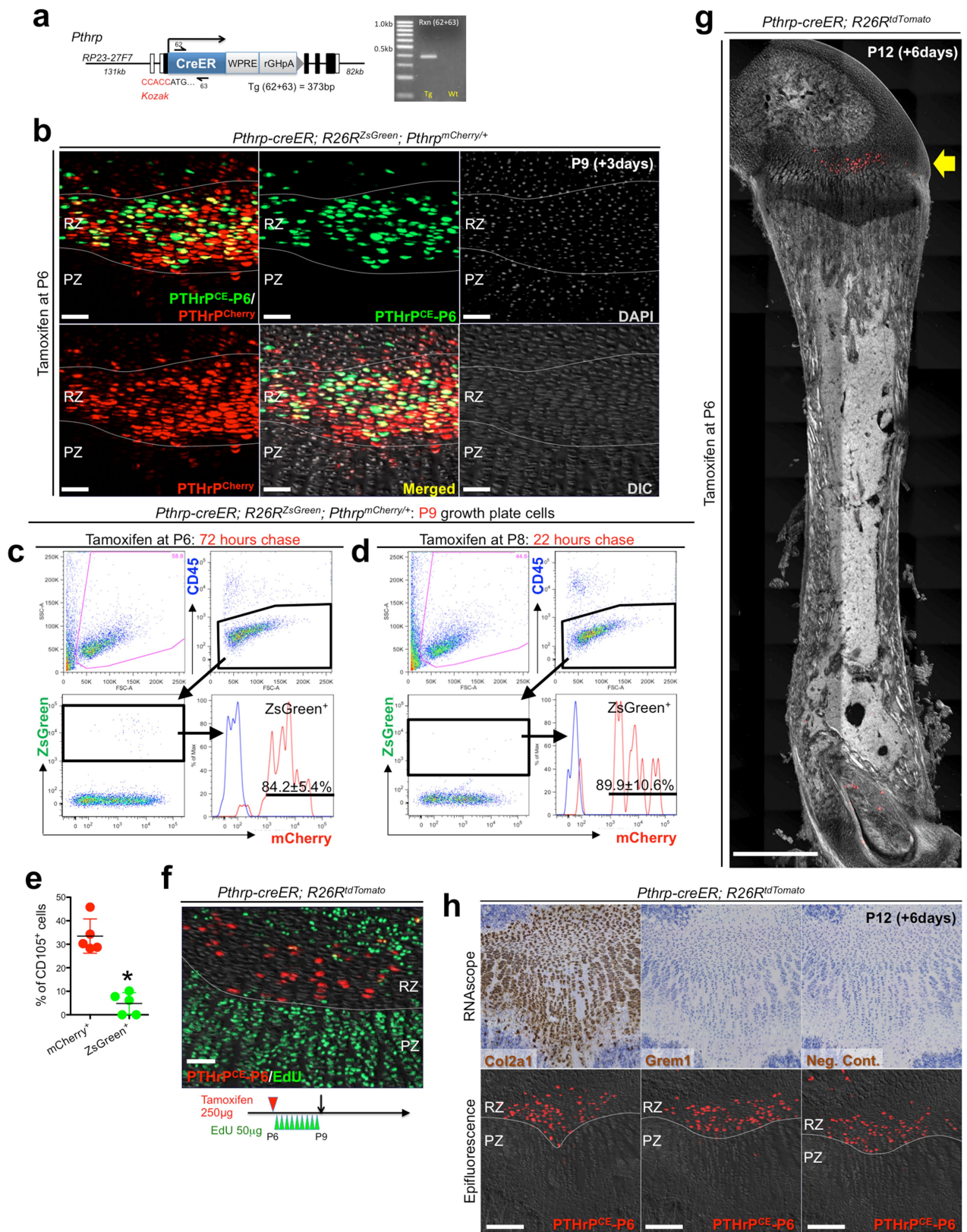
Extended Data Fig. 1 | Generation and characterization of *Pthrp*-*mCherry* knock-in allele. a, CRISPR-Cas9 generation of *Pthrp*-*mCherry* knock-in allele. Structure of the genomic *Pthrp* locus, targeting vector and knock-in allele after homologous recombination. White boxes, untranslated region; black boxes, coding region; ex, exon. Blue bars, homology arms; red bars, guide RNAs (gRNAs) as part of CRISPR-Cas9 reagents; red boxes, *Kozak*-*mCherry*-*bGHpA* cassette replacing the native start codon. Half arrows, primers; wild-type forward (289), wild-type reverse (290) and mutant reverse (291). Bottom, PCR genotyping using 289, 290 and 291 primer mix; wild-type (WT) allele, 185 bp; knock-in

(KI) allele, 385 bp. At least $n = 100$ independent experiments with similar results. **b**, *Pthrp*^{*mCherry*/+} fetal distal femurs with EdU administration shortly before analysis (3 h). Bottom panels show magnified views of perichondrium. Dotted lines, borders of bone anlage. Grey, DAPI and DIC. Scale bars, 200 μm (top panels), 100 μm (bottom panels). $n = 2$ (E13.5, E15.5) mice, $n = 1$ (α -Sox9) mouse. **c**, *Pthrp*^{*mCherry*/+} distal-femur growth plates with EdU administration shortly before analysis (3 h). Bottom panels show magnified views of central growth plates. Arrowheads, *mCherry*⁺ cells. Grey, DAPI and DIC. Scale bars, 200 μm (top panels), 50 μm (bottom panels).



Extended Data Fig. 2 | Skeletal stem and progenitor cell-marker expression in PTHrP-mCherry⁺ resting chondrocytes. **a**, Flow cytometry analysis of *Pthrp*^{mCherry/+} growth-plate cells (top panels) and bone-marrow cells (bottom panels). $n = 8$ mice for *Pthrp*^{mCherry/+} and $n = 3$ mice for *Pthrp*^{+/+}, data are presented as mean \pm s.d. **b**, Flow cytometry analysis of *Col1a1(2.3kb)-GFP; Pthrp*^{mCherry/+} growth-plate cells. $n = 5$ mice per group, data are presented as mean \pm s.d. **c**, Skeletal stem and progenitor cell-surface-marker analysis of *Pthrp*^{mCherry/+} growth-plate cells. Unstained, *Pthrp*^{+/+} cells mice only stained for CD45, Ter119 and CD31; mCherry⁻, mCherry⁺ fraction of *Pthrp*^{mCherry/+} cells;

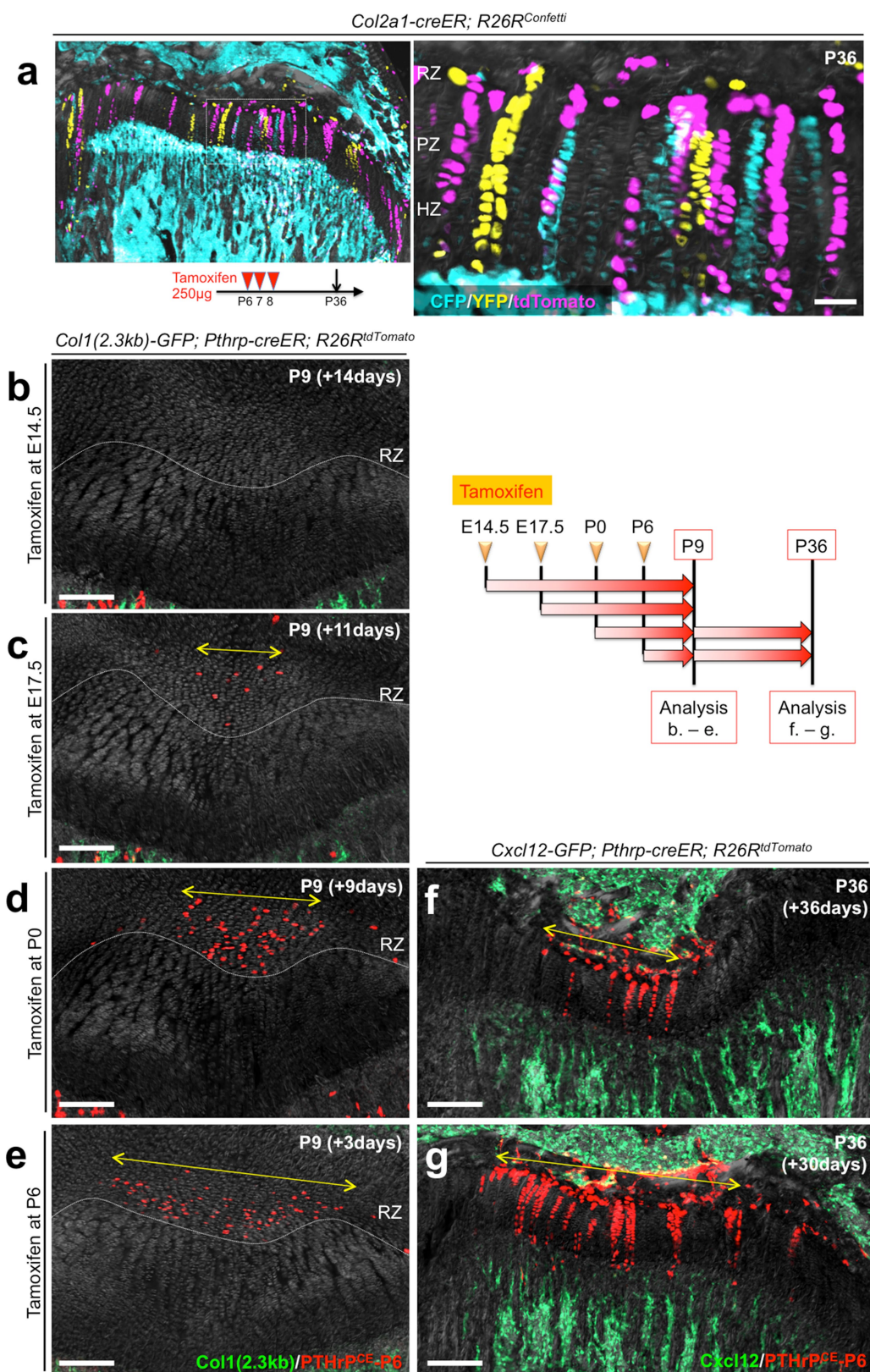
mCherry⁺, mCherry⁺ fraction of *Pthrp*^{mCherry/+} cells. Magenta box, CD45⁻Ter119⁻CD31⁻CD51⁺CD90⁻mCherry⁺ fraction. $n = 3$ mice for *Pthrp*^{mCherry/+}, data are presented as mean \pm s.d., $n = 1$ mouse for *Pthrp*^{+/+}. **d**, Composition of CD45⁻Ter119⁻CD31⁻mCherry⁺ growth-plate cells. $n = 3$ mice per group, data are presented as mean \pm s.d. **e**, Percentage of mCherry⁺ cells among mSSCs (left, CD105⁻CD200⁺), pre-BCSPs (centre, CD105⁻CD200⁻) and BCSPs (right, CD105⁺), gated under CD45⁻Ter119⁻CD31⁻CD51⁺CD90⁻ fraction. $n = 3$ mice per group, data are presented as mean \pm s.d.



Extended Data Fig. 3 | See next page for caption.

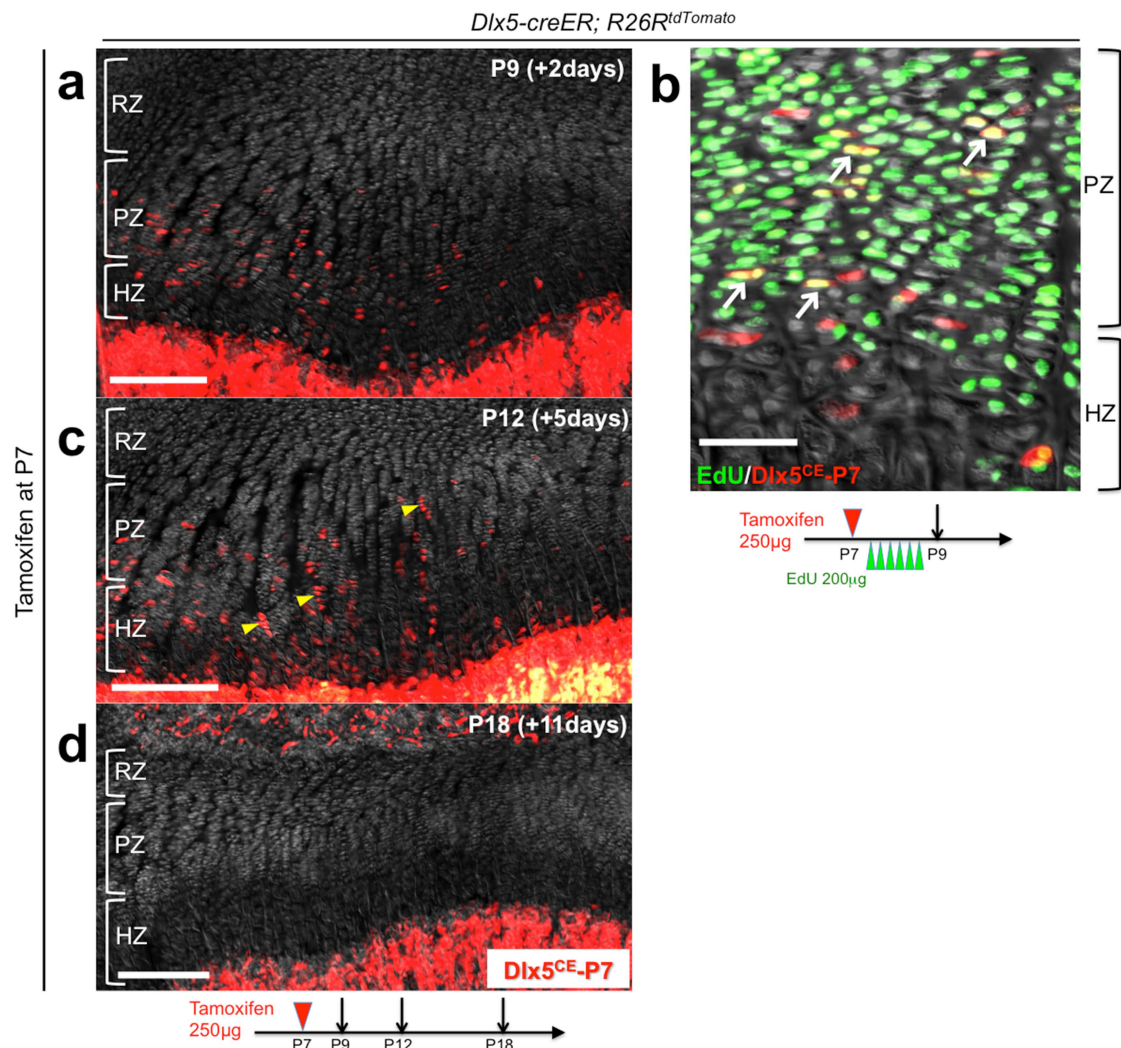
Extended Data Fig. 3 | Generation and characterization of *Pthrp-creER* bacterial artificial chromosome transgenic line. **a**, Generation of *Pthrp-creER* bacterial artificial chromosome (BAC) transgenic mice. Structure of the *Pthrp-creER-WPRE-rGHpA* BAC construct. *Kozak-Pthrp-creER-WPRE-rGHpA-frt-Neo^R-frt* cassette containing 62-bp homology arms was recombineered into a BAC clone RP23-27F7 containing 131-kb upstream and 82-kb downstream genomic sequences of the *Pthrp* gene. *Neo^R* and backbone *lox* sites were removed before pronuclear injection. Half arrows, forward (62) and reverse (63) primers. Right, PCR genotyping using 62 and 63 primer mix; transgenic (Tg), 373 bp. White boxes, exons; black boxes, introns. At least $n = 100$ independent experiments with similar results. **b**, Short-chase analysis of *Pthrp-creER;R26R^{ZsGreen};Pthrp^{mCherry/+}* distal-femur growth plates (pulsed on P6). Scale bars, 50 μm . $n = 3$ mice. **c–e**, Short-chase flow cytometry analysis of *Pthrp-creER;R26R^{ZsGreen};Pthrp^{mCherry/+}* growth-plate cells, with tamoxifen injection at 72 h (**c**, **e**) or 22 h (**d**) in advance. Red lines, ZsGreen⁺ cells;

blue lines, control cells without PTHrP-mCherry. $n = 5$ mice (72 h) or $n = 3$ mice (22 h) per group. **e**, Percentage of CD105⁺ cells within mCherry⁺ (red) and ZsGreen⁺ (green) cells. $n = 5$ mice per group, data are presented as mean \pm s.d., $*P = 0.012$, Mann–Whitney's *U*-test, two-tailed. **f**, *Pthrp-creER;R26R^{tdTomato}* distal-femur growth plates (pulsed on P6) at P9. EdU (50 μg) was serially injected 9 times at 8-h intervals between P6 and P9. Grey, DIC. Scale bars: 50 μm . $n = 3$ mice. **g**, Scanning of *Pthrp-creER;R26R^{tdTomato}* whole femur (pulsed on P6) at P12. Arrow, tdTomato⁺ cells localized within the resting zone of distal femur. Grey, DAPI and DIC. Scale bars, 1 mm. $n = 3$ mice. **h**, High sensitivity in situ hybridization (RNAscope) analysis of *Pthrp-creER;R26R^{tdTomato}* distal-femur growth plates (pulsed on P6) at P12. Top and bottom panels represent the identical section, before (bottom panels) and after (top panels) hybridization. Left panels, *Col2a1* (positive control); centre panels, *Grem1*; right panels, negative control. Grey, DAPI and DIC. Scale bars, 200 μm . $n = 3$ independent experiments.



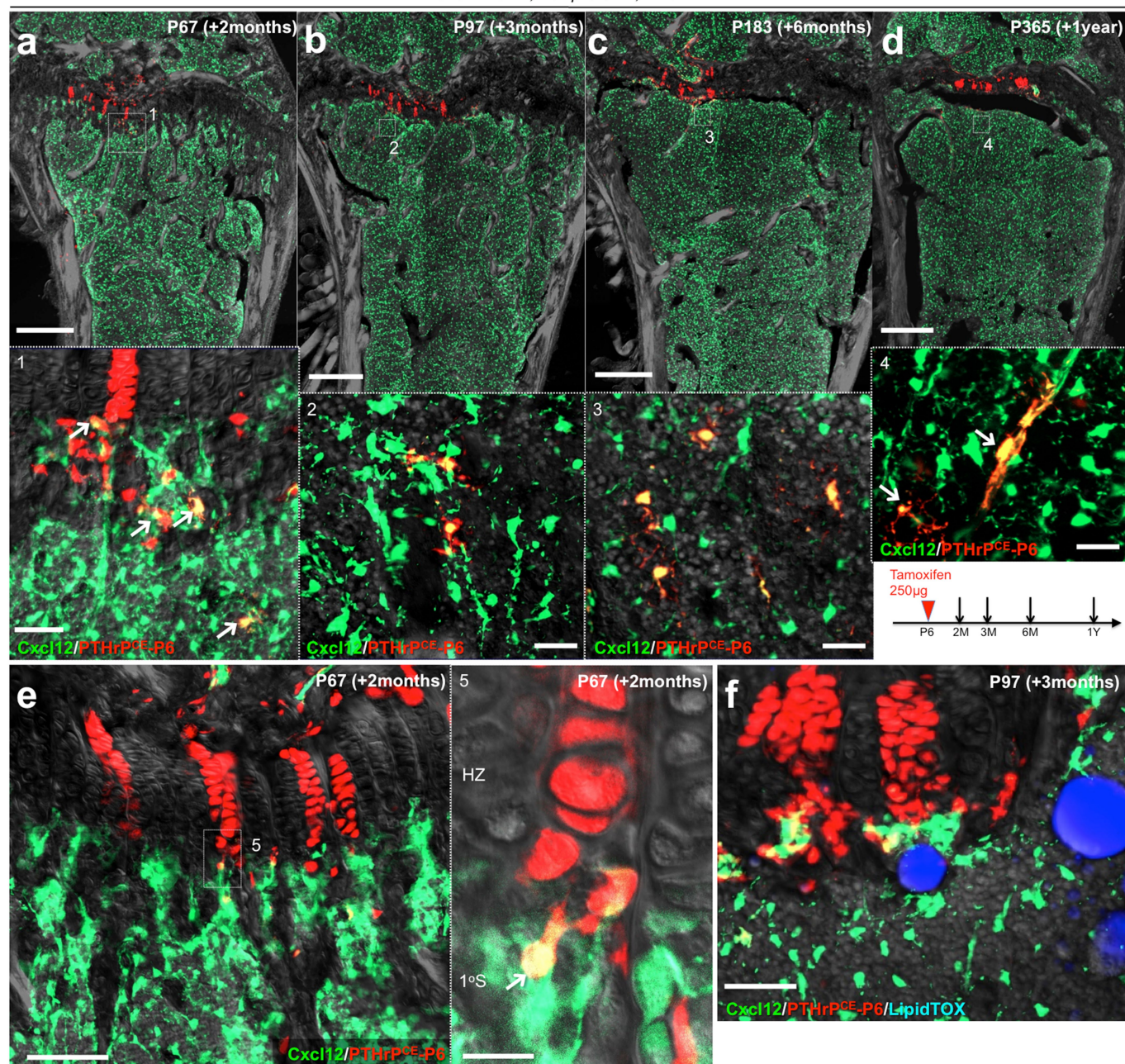
Extended Data Fig. 4 | PTHrP⁺ resting chondrocytes are functionally dedicated to columnar chondrocyte formation. **a**, In vivo clonal analysis of *Col2a1-creER⁺* growth-plate chondrocytes. *Col2a1-creER;R26R^{Confetti}* distal-femur growth plates (pulsed on P6, P7 and P8). Scale bars, 50 µm. *n* = 2 mice. **b–e**, *Col1a1(2.3kb)-GFP;Pthrp-creER;R26R^{tdTomato}* distal-femur growth plates, shown at P9 after being pulsed at various preceding

time points. Yellow double-headed arrows, *tdTomato⁺* domain within the resting zone. Grey, DAPI and DIC. Scale bars, 200 µm. *n* = 3 mice per group. **f, g**, *Cxcl12-GFP;Pthrp-creER;R26R^{tdTomato}* distal-femur growth plates, shown at P36 after being pulsed on P0 (**f**) and P6 (**g**). Yellow double-headed arrows in **f, g** indicate the same width as those shown in **d, e**. Grey, DAPI and DIC. Scale bars, 200 µm. *n* = 3 mice per group.



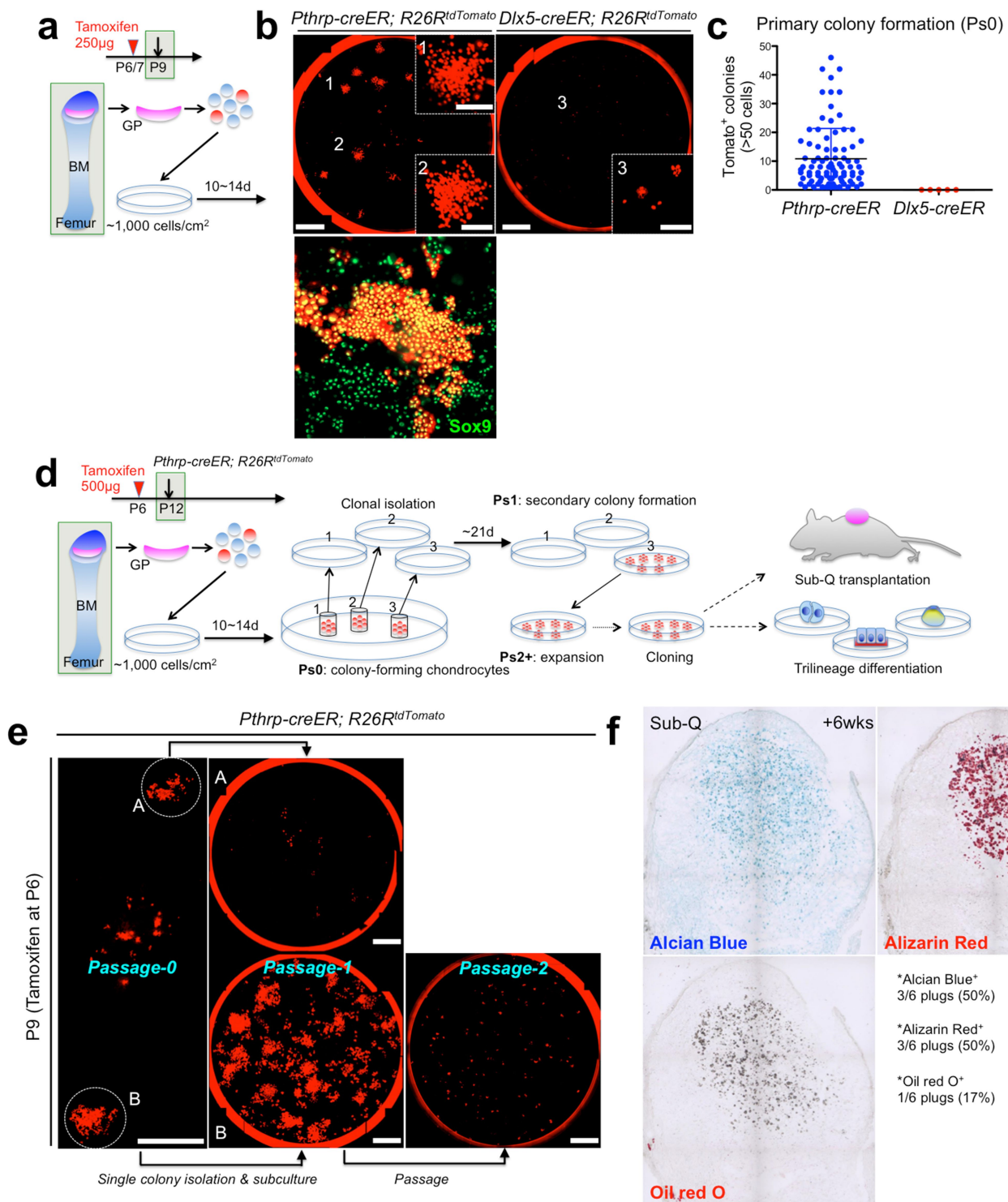
Extended Data Fig. 5 | *Dlx5-creER*⁺ proliferating chondrocytes are not the source of columnar chondrocytes. **a–d**, Cell-fate analysis of *Dlx5-creER*⁺ proliferating chondrocytes. *Dlx5-creER;R26R^{tdTomato}* distal-femur growth plates (pulsed on P7). **b**, EdU (200 µg) was serially injected

6 times at 8-h intervals, between P7 and P9. Arrows, EdU⁺tdTomato⁺ cells; arrowheads, short columns (<10 cells). Grey, DAPI and DIC. Scale bars, 200 µm (left panels), 50 µm (right panel). *n* = 3 mice at each time point.

Cxcl12-GFP; Pthrp-creER; R26R^{tdTomato}

Extended Data Fig. 6 | *Pthrp-creER*⁺ resting chondrocytes are precursors for bone marrow reticular stromal cells. *Cxcl12-GFP;Pthrp-creER;R26R^{tdTomato}* distal femurs (pulsed on P6). a–d, Bottom panels show magnified views of the dotted areas beneath growth plates. Arrows, *Cxcl12-GFP*⁺*tdTomato*⁺ reticular stromal cells. e, Magnified view of the junction between hypertrophic layer and primary spongiosa. Arrow, *Cxcl12-GFP*⁺*tdTomato*⁺ reticular stromal cells immediately below the

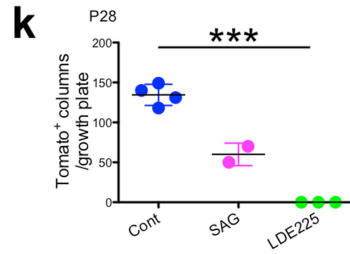
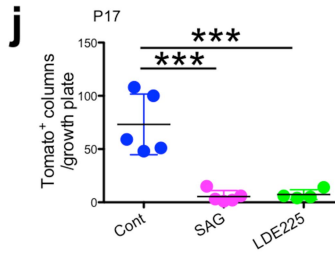
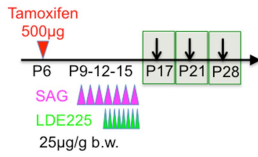
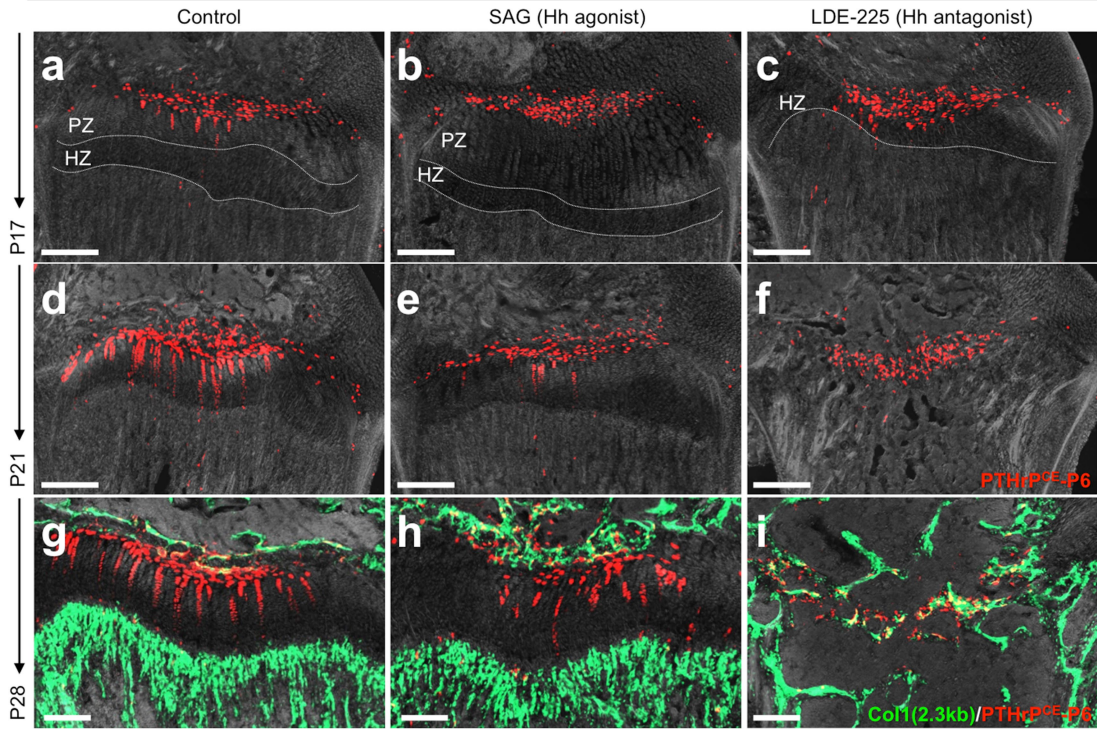
hypertrophic zone. 1°S: primary spongiosa. f, Magnified view of the metaphyseal bone marrow. Mice were fed with high-fat diet containing rosiglitazone between P56 and P97. Grey, DAPI and DIC. Scale bars, 500 μ m (a–d, f), 100 μ m (e), 50 μ m (bottom panels of a–c), 20 μ m (bottom panel of d, right panel of e). $n = 3$ mice for each group, except $n = 2$ mice for P365.



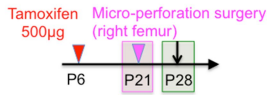
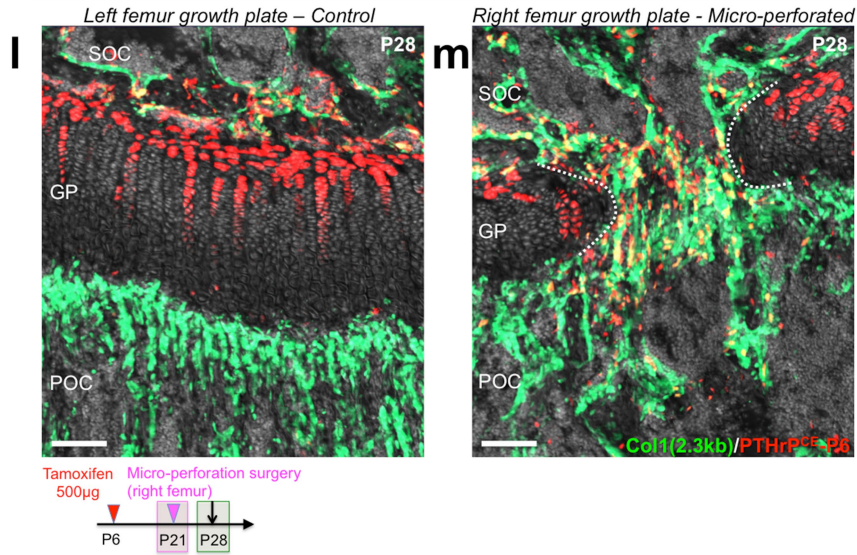
Extended Data Fig. 7 | *Pthrp-creER*⁺ resting chondrocytes uniquely possess colony-forming capabilities ex vivo. **a**, Diagram of colony-forming assay. Growth-plate cells were isolated from *Pthrp-creER;R26R^{tdTomato}* (pulsed on P6) or *Dlx5-creER;R26R^{tdTomato}* (pulsed on P7) mice at P9, and cultured at a clonal density ($\sim 1,000$ cells per cm^2) for 10–14 days to initiate colony formation. BM, bone marrow. **b**, Colony-forming assay. Left top, *Pthrp-creER;R26R^{tdTomato}*; right, *Dlx5-creER;R26R^{tdTomato}*. Insets 1, 2 and 3 show magnified views of the corresponding areas (labelled with 1, 2, 3). Bottom left, Sox9 staining of primary *Pthrp-creER* tdTomato⁺ colonies. Red, tdTomato. Scale bars, 5 mm (top panels), 1 mm (top panel insets), 200 μm (bottom panel). $n = 88$ mice for *Pthrp-creER;R26R^{tdTomato}*, $n = 5$ for *Dlx5-creER;R26R^{tdTomato}*.

c, Quantification of tdTomato⁺ colonies (>50 cells) established from *Pthrp-creER;R26R^{tdTomato}* ($n = 88$) and *Dlx5-creER;R26R^{tdTomato}* ($n = 5$) mice. Data are presented as mean \pm s.d. **d**, Diagram of colony-forming assay and subsequent analyses on self-renewal, trilineage differentiation and transplantation of individual colony-forming cells. **e**, Isolation of single PTHrP^{CE}-tdTomato⁺ colonies and subsequent subculture of isolated clones. A, exhausting clone; B, self-renewing clone establishing secondary colonies. Right, clone B did not proliferate at passage 2 upon bulk culture. Red, tdTomato. Scale bars, 5 mm. $n = 518$ independent experiments. **f**, Subcutaneous transplantation of PTHrP^{CE}-tdTomato⁺ clones into immunodeficient mice. $n = 8$ mice.

Pthrp-creER; R26R^{tdTomato} (Tamoxifen at P6)



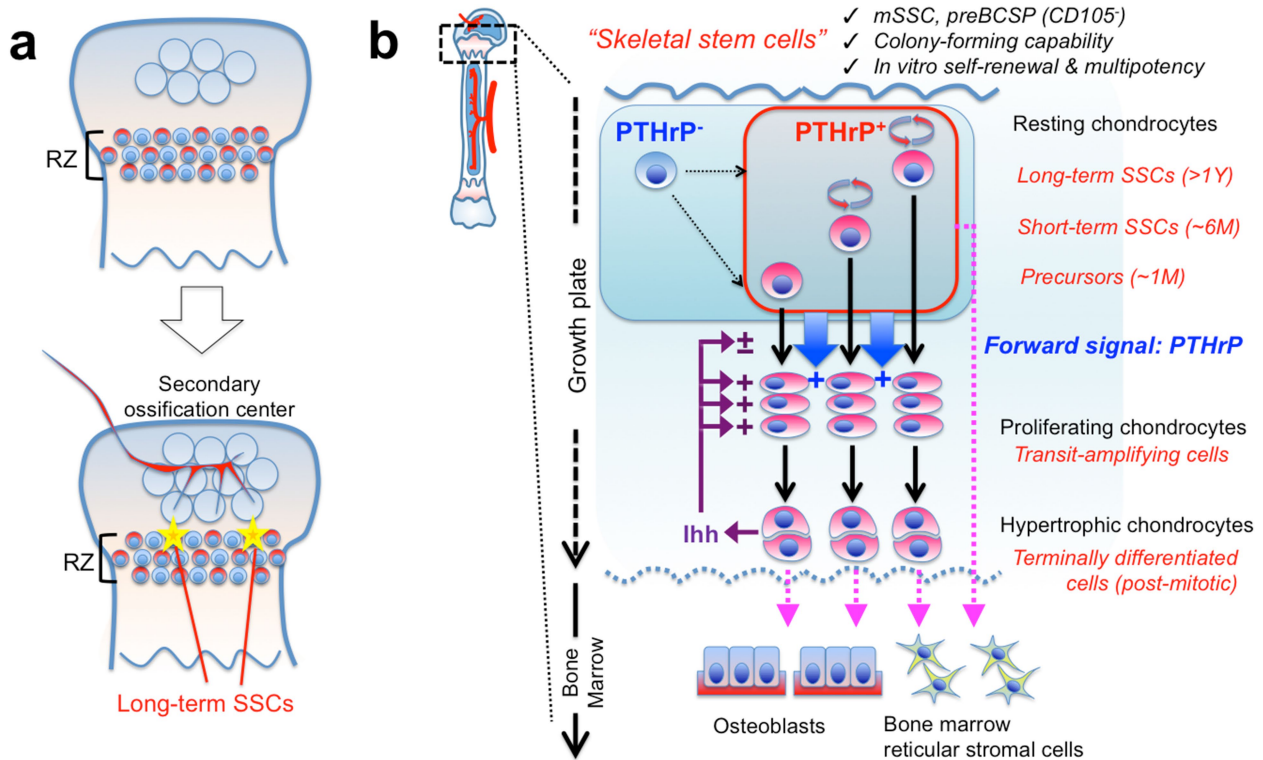
Col1(2.3kb)-GFP; Pthrp-creER; R26R^{tdTomato}: P28 (Tamoxifen at P6, Surgery at P21)



Extended Data Fig. 8 | See next page for caption.

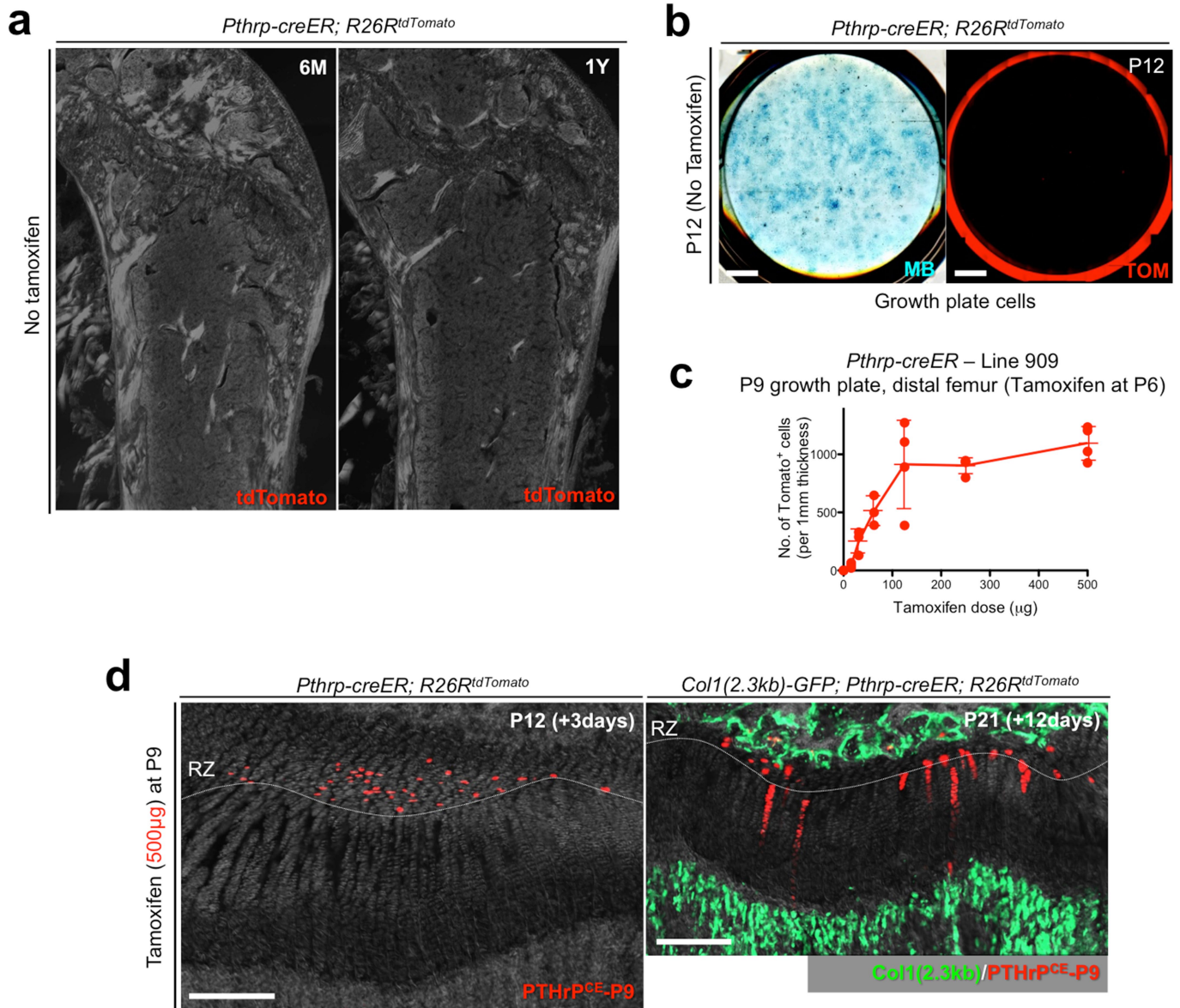
Extended Data Fig. 8 | *Pthrp-creER*⁺ resting chondrocytes form columnar chondrocytes in a Hedgehog-responsive, niche-dependent manner. **a–i**, Pharmacological manipulation of Hedgehog signalling. *Pthrp-creER;R26R^{tdTomato}* distal-femur growth plates (pulsed on P6). Left panels, vehicle control; centre panels, SAG (Hh agonist)-treated samples; right panels, LDE225 (Hh antagonist)-treated samples. Grey, DAPI and DIC. Scale bars, 200 μm . **j, k**, Quantification of tdTomato⁺ columns in *Pthrp-creER;R26R^{tdTomato}* distal-femur growth plates (pulsed on P6). P17, $n = 5$ (control), $n = 5$ (SAG), $n = 4$ (LDE225) mice per group. P28, $n = 4$ (control), $n = 3$ (LDE225) mice per group. Data are presented as mean \pm s.d. P28, $n = 2$ (SAG). *** $P < 0.001$; P17 control versus SAG,

mean difference = 67.8, 95% confidence interval (37.5, 98.1); P17 control versus LDE225, mean difference = 66.0, 95% confidence interval (33.9, 98.0); P17 SAG versus LDE225, mean difference = -1.85, 95% confidence interval (-33.9, 30.2); P28 control versus LDE225, mean difference = 134.5, 95% confidence interval (108.7, 160.3). One-way ANOVA followed by Tukey's multiple comparison test. **l, m**, Micro-perforation injury of growth plates. *Col1a1(2.3kb)-GFP;Pthrp-creER;R26R^{tdTomato}* distal femurs (pulsed on P6) at P28. Micro-perforation surgery was performed at P21. **l**, Left femur growth plate (control). **m**, Right femur growth plate (micro-perforated). Dotted line, micro-perforated area. Grey, DAPI and DIC. Scale bars, 100 μm . $n = 3$ mice.



Extended Data Fig. 9 | Resting zone of the growth plate contains a unique class of skeletal stem cells. **a**, Formation of PTHrP⁺ skeletal stem cells within the growth plate. A small subset of PTHrP⁺ chondrocytes in the resting zone acquire properties as long-term skeletal stem cells in conjunction with the formation of the highly vascularized secondary ossification centre. **b**, PTHrP⁺ skeletal stem cells are heterogeneously composed of long-term, short-term and transient populations, and undergo asymmetric divisions and maintain themselves within the

resting zone. These cells may be supplemented by PTHrP⁻ cells. PTHrP⁺ cells perform two different functions: (1) these cells differentiate into proliferating chondrocytes, hypertrophic chondrocytes and eventually become osteoblasts and bone marrow stromal cells at the post-mitotic stage. (2) These cells send a forward signal (PTHrP) to control chondrocyte proliferation and differentiation. Indian hedgehog (Ihh) secreted by hypertrophic chondrocytes maintains the proliferation of chondrocytes and formation of columnar chondrocytes.



Extended Data Fig. 10 | Absence of tamoxifen-independent recombination in *Pthrp-creER* line. **a**, No tamoxifen controls of *Pthrp-creER;R26R^{tdTomato}* mice at 6 months (left) and 1 year (right) of age. Red, tdTomato; blue, DAPI; grey, DIC. Scale bars, 500 μm. $n = 3$ mice per group. **b**, No tamoxifen controls of primary colonies (passage 0) isolated from *Pthrp-creER;R26R^{tdTomato}* mice at P12 without tamoxifen injection. Left, methylene blue (MB) staining; right, red tdTomato (TOM). Scale bar, 5 mm. $n = 3$ mice. **c**, Dose–response curve of recombination based on *Pthrp-creER*. Quantification of tdTomato⁺ cells in resting zone at P9 in

Pthrp-creER;R26R^{tdTomato} mice upon a single dose of tamoxifen at P6. x axis, dose of tamoxifen (μg); y axis, the number of tdTomato⁺ cells per 1-mm thickness. $n = 3$ (0, 31.3 and 62.5 μg), $n = 4$ (15.6, 125, 250 and 500 μg) mice per group, data are presented as mean \pm s.d. **d**, Tamoxifen-induced recombination in growth plates pulsed on P9. *Pthrp-creER;R26R^{tdTomato}* distal-femur growth plates at P12 (left) and *Col1a1(2.3kb)-GFP; Pthrp-creER;R26R^{tdTomato}* mice at P21 (right). Tamoxifen (500 μg) was injected at P9. Green, Col1a1(2.3kb)-GFP; red, tdTomato; grey, DAPI and DIC. Scale bars, 200 μm. $n = 3$ mice.

Reporting Summary

Nature Research wishes to improve the reproducibility of the work that we publish. This form provides structure for consistency and transparency in reporting. For further information on Nature Research policies, see [Authors & Referees](#) and the [Editorial Policy Checklist](#).

Statistical parameters

When statistical analyses are reported, confirm that the following items are present in the relevant location (e.g. figure legend, table legend, main text, or Methods section).

n/a Confirmed

- The exact sample size (n) for each experimental group/condition, given as a discrete number and unit of measurement
- An indication of whether measurements were taken from distinct samples or whether the same sample was measured repeatedly
- The statistical test(s) used AND whether they are one- or two-sided
Only common tests should be described solely by name; describe more complex techniques in the Methods section.
- A description of all covariates tested
- A description of any assumptions or corrections, such as tests of normality and adjustment for multiple comparisons
- A full description of the statistics including central tendency (e.g. means) or other basic estimates (e.g. regression coefficient) AND variation (e.g. standard deviation) or associated estimates of uncertainty (e.g. confidence intervals)
- For null hypothesis testing, the test statistic (e.g. F , t , r) with confidence intervals, effect sizes, degrees of freedom and P value noted
Give P values as exact values whenever suitable.
- For Bayesian analysis, information on the choice of priors and Markov chain Monte Carlo settings
- For hierarchical and complex designs, identification of the appropriate level for tests and full reporting of outcomes
- Estimates of effect sizes (e.g. Cohen's d , Pearson's r), indicating how they were calculated
- Clearly defined error bars
State explicitly what error bars represent (e.g. SD, SE, CI)

Our web collection on [statistics for biologists](#) may be useful.

Software and code

Policy information about [availability of computer code](#)

Data collection ZEN 2 (blue edition, ZEISS), FACSDiva v8.0.1 (BD)

Data analysis Image J (NIH), FlowJo 9.3.3 (TreeStar), GraphPad Prism 5.0

For manuscripts utilizing custom algorithms or software that are central to the research but not yet described in published literature, software must be made available to editors/reviewers upon request. We strongly encourage code deposition in a community repository (e.g. GitHub). See the Nature Research [guidelines for submitting code & software](#) for further information.

Data

Policy information about [availability of data](#)

All manuscripts must include a [data availability statement](#). This statement should provide the following information, where applicable:

- Accession codes, unique identifiers, or web links for publicly available datasets
- A list of figures that have associated raw data
- A description of any restrictions on data availability

The figure source data were provided in the supplementary information file. The datasets generated during and/or analyzed during the current study are available in Dryad Digital Repository (<https://datadryad.org>) with the identifier doi:10.5061/dryad.3qq5bm7.

Field-specific reporting

Please select the best fit for your research. If you are not sure, read the appropriate sections before making your selection.

Life sciences Behavioural & social sciences Ecological, evolutionary & environmental sciences

For a reference copy of the document with all sections, see [nature.com/authors/policies/ReportingSummary-flat.pdf](https://www.nature.com/authors/policies/ReportingSummary-flat.pdf)

Life sciences study design

All studies must disclose on these points even when the disclosure is negative.

Sample size	No statistical method was used to predetermine sample size. We chose the numbers of mice to study based on our prior experience that give good standard errors of the mean and good statistics to make it unlikely that we miss a biologically important difference between groups.
Data exclusions	Some of the data were excluded from the study because of the pre-established criteria such as problems or failures in identifying correct genotypes or birth dates, and issues unrelated to the intervention of the study such as spontaneous malnutrition. In any case, we consistently used littermate controls with corresponding genotypes in analysis.
Replication	For all data presented in the manuscript, we examined at least three independent biological samples (three different mice) to ensure the reproducibility. For each series of the experiments, all attempts at replication were successful.
Randomization	The experiments were not randomized. We used all the available mice of the desired genotypes. Mice were allocated to particular groups based on results of PCR-genotyping typically performed around one week after birth. Covariates were controlled by considering multiple factors, such as genotypes and general phenotypical data (i.e. body weight). On principle, we did not observe any particular difference among groups.
Blinding	The investigators were not blinded to allocation during experiments and outcome assessment because it was impossible due to following reasons: samples were allocated to particular groups before experiments were initiated based on genotyping results, and given unique identifiers highlighting groups throughout experiments i.e. housing in cages, tissue collections, sample preparation and data acquisition. However, we did not pay particular attention to groups when we were measuring and counting.

Reporting for specific materials, systems and methods

Materials & experimental systems

n/a	Involvement in the study
<input type="checkbox"/>	<input checked="" type="checkbox"/> Unique biological materials
<input type="checkbox"/>	<input checked="" type="checkbox"/> Antibodies
<input checked="" type="checkbox"/>	<input type="checkbox"/> Eukaryotic cell lines
<input checked="" type="checkbox"/>	<input type="checkbox"/> Palaeontology
<input type="checkbox"/>	<input checked="" type="checkbox"/> Animals and other organisms
<input checked="" type="checkbox"/>	<input type="checkbox"/> Human research participants

Methods

n/a	Involvement in the study
<input checked="" type="checkbox"/>	<input type="checkbox"/> ChIP-seq
<input type="checkbox"/>	<input checked="" type="checkbox"/> Flow cytometry
<input checked="" type="checkbox"/>	<input type="checkbox"/> MRI-based neuroimaging

Unique biological materials

Policy information about [availability of materials](#)

Obtaining unique materials There is no restriction on availability of unique materials (genetically engineered mice) used for this study. These mice will be deposited at a repository upon publication.

Antibodies

Antibodies used

ThermoFisher/eBioscience
 eFlour450-conjugated CD31 (390, Cat# 48-0311-82, Lot# 4301770)
 eFlour450-conjugated CD45 (30F-11, Cat# 48-0451-82, Lot # 4295770)
 eFlour450-conjugated Ter119 (TER-119, Cat# 48-5921-82, Lot# 4295840)
 Fluorescein isothiocyanate (FITC)-conjugated CD90.2 (30-H12, Cat# 11-0903-81, Lot# E00428-1634)
 Phycoerythrin (PE)-conjugated CD51 (RMV-7, Cat# 12-0512-81, Lot# E01293-1633)
 Allophycocyanin (APC)-conjugated CD105 (MJ7/18, Cat# 17-1051-80, Lot# 24407-101)
 Peridinin chlorophyll protein complex (PerCP)-eFlour710-conjugated CD200 (OX90, Cat# 46-5200-80, Lot# 4298110).

ThermoFisher/Invitrogen
 Alexa Fluor 488 goat anti-rabbit IgG (H+L) (Cat# A11034, Lot760000)
 Alexa Fluor 647 donkey anti-rabbit IgG (H+L) (Cat# A31573, Lot1322326)
 Alexa Fluor 647 donkey anti-goat IgG (H+L) (Cat# A21447, Lot1301819)

EMD-Millipore
 Rabbit anti-Sox9 polyclonal antibody (Cat# AB5535, Lot# 2847051, 2922429)

R&D systems
 Goat anti-osteopontin (OPN) polyclonal antibody (Cat# AF808, Lot# 0615081, 0617041)

Validation

More detailed information about these antibodies is available on these manufacturers' websites.

Animals and other organisms

Policy information about [studies involving animals](#); [ARRIVE guidelines](#) recommended for reporting animal research

Laboratory animals

We used genetically modified mice (*mus musculus*) for this study. Most of the mouse lines have been backcrossed to a C57/BL6 background. We used female breeder mice in a FVB/N background. Mice with both sexes were used throughout their lifespan (up to 2 years of age). Mouse strains used in the study were as following: PTHrP-creERT2-WPRE, PTHrP-mCherry/null, Cxcl12-GFP/null, Col1a1(2.3kb)-GFP (JAX013134), Dlx5-creERT2 (JAX010705), Col2a1-creERT2 (JAX006774), Rosa26-CAG-loxP-stop-loxP-tdTomato (Ai14: R26R-tdTomato, JAX007914), Rosa26-CAG-loxP-stop-loxP-ZsGreen (Ai6: R26R-ZsGreen, JAX007906), Rosa26-SALoxP-stop-loxP-DTA (ROSA-DTA, JAX009669) and Rosa26-CAG-loxP-stop-loxP-Confetti (R26R-Confetti, JAX013731), NOD scid gamma (NSG) (JAX005557).

Wild animals

N/A

Field-collected samples

N/A

Flow Cytometry

Plots

Confirm that:

- The axis labels state the marker and fluorochrome used (e.g. CD4-FITC).
- The axis scales are clearly visible. Include numbers along axes only for bottom left plot of group (a 'group' is an analysis of identical markers).
- All plots are contour plots with outliers or pseudocolor plots.
- A numerical value for number of cells or percentage (with statistics) is provided.

Methodology

Sample preparation

Distal epiphyses of femurs were manually dislodged, and attached soft tissues and woven bones were carefully removed using forceps. Dissected epiphyses were incubated with 2 Wunsch units of Liberase TM (Roche) in 3ml Ca²⁺, Mg²⁺-free Hank's Balanced Salt Solution (HBSS, Sigma H6648) at 37°C for 60 min on a shaking incubator (ThermomixerR, Eppendorf). After this initial digestion, remaining surrounding soft tissues, including perichondrium and hypertrophic layers, were removed by rolling epiphyses over sterile paper towels (Scott C-fold towels, Kimberly-Clark) for several times. Articular cartilage and secondary ossification centers were subsequently removed. Dissected growth plates were minced using a disposable scalpel (No.15, Graham-Field), and further incubated with Liberase TM at 37°C for 60 min on a shaking incubator. Cells were mechanically triturated using an 18-gauge needle and a 1ml Luer-Lok syringe (BD), and filtered through a 70µm cell strainer (BD) into a 50ml tube on ice to single cell suspension. After washing, tissue remnants were incubated with Liberase TM at 37°C for 30 min on a shaking incubator, and cells were filtered into the same tube. Cells were pelleted and resuspended in appropriate medium for flow cytometry.

Instrument

BD LSR Fortessa (BDBiosciences)

Software

FACSDiva v8.0.1 (BD) & FlowJo 9.3.3 (TreeStar) software

Cell population abundance

N/A

Gating strategy

Single cells were first gated using FSC and SSC denominators. Only CD45 negative fraction was gated and analyzed. Negative 'unstained' control samples were always used as a reference to determine the demarcation between the positive and negative populations.

- Tick this box to confirm that a figure exemplifying the gating strategy is provided in the Supplementary Information.